# Cortical involvement of slow wave activity predicts scene memory: a PCA-approach to memory consolidation

Student: Albert Serweta
1951637
Bachelor Thesis
8th of July 2020

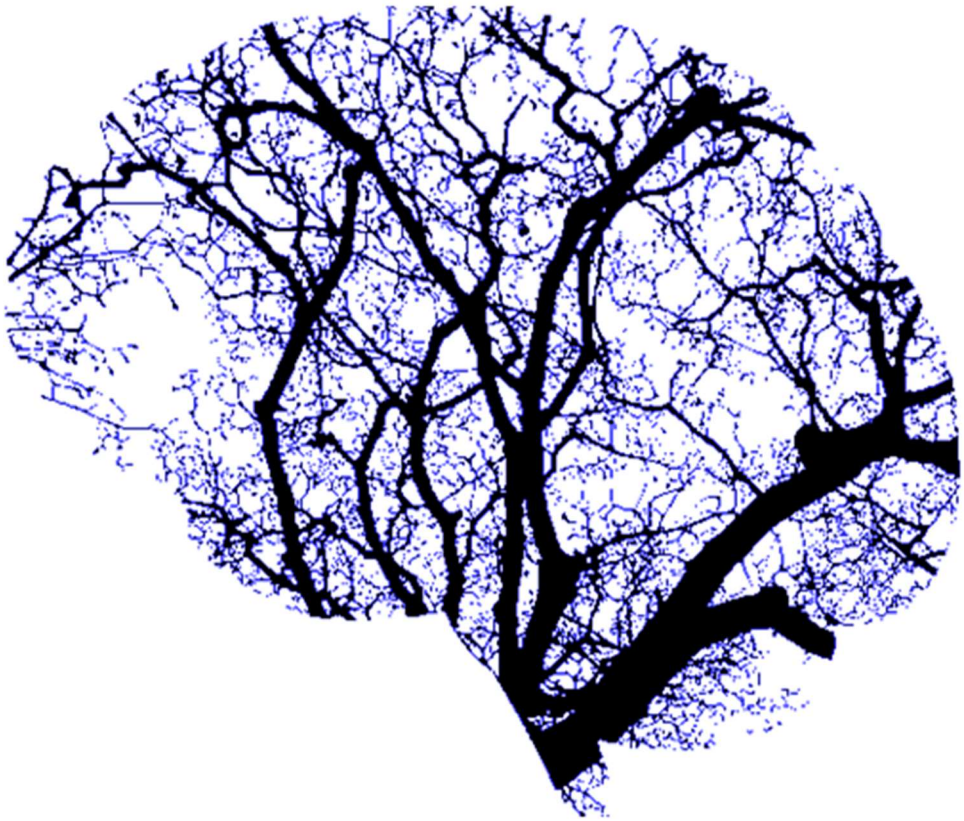

University of Twente
Faculty of Cognitive Psychology and Ergonomics
Subject: Psychology
Bachelor Thesis
Supervisor: Rob van der Lubbe
Second Supervisor: Frank van der Velde

## Table of Contents



Cover source: https://donecountingsheep.com/2019/04/05/how-does-poor-sleep-affect-the-brain/

**Abstract**

Slow wave activity (0.5-4 Hz) has been linked consistently to memory consolidation during sleep. Interestingly, slow waves types can be delineated on the basis of distinct synchronization mechanisms: 1) arousal-dependent synchronization, yields large, Type 1 slow waves, and 2) a homeostatic, cortico-cortical mechanism, synchronizes smaller, Type 2 slow waves. Memory consolidation or learning-dependent adjustments of neural connections during sleep are mainly associated with such local, homeostatic events.

Conventionally, sleep-dependent effects of slow wave activity on memory were examined with measures of power or power density. Considering anterior predominance of large, Type 1 slow waves, power-based measures may fail to capture learning-dependent/homeostatic changes in incidence of smaller, Type 2 slow waves. The present study introduced cortical involvement of slow wave activity, by means of spatial, principal component analyses (PCA), as a novel approach to study memory consolidation during sleep.

To this end, a high-density EEG dataset was utilized. Participants performed a subsequent memory paradigm, using real-life sceneries, then they took a nap upon which they performed a scene recognition task. Effects of cortical involvement of slow wave activity on scene recognition were assessed. In addition, conventional analyses of slow wave power were performed to validate the novel approach. Against the background of fronto-central power predominance, robust memory correlates of both parieto-central involvement and power of slow waves were found during nap sleep. Thus, spatial PCA may provide a novel tool to assess learning-dependent changes in cortical involvement of slow wave activity and relate these to memory consolidation processes.

**Keywords:** sleep, memory, learning, EEG, sleep homeostasis, scene recognition

## 1. Introduction

The enterprise to understand the mechanisms of human memory dates back more than a century to Müller and Pilzecker (1900). They were the first to propose that newly acquired memories undergo a physiological process, termed consolidation, that preserves memories over time and prevents their deterioration. However, acquisition and consolidation of memory appear to depict two opposing processes. Arousal and alertness benefit the former. But as myriads of sleep and sleep deprivation studies made undoubtedly clear, we also need to go "offline" in order to consolidate and store what we have learned (Dudai, Karni, & Born, 2015; Curcio, Ferrara, & De Gennaro, 2006; Drummond et al., 2000). Freed from processing of ongoing experience, sleep provides an optimal milieu for our brains to sample newly acquired information against the background of prior knowledge. Such comprehensive sampling of past experience should account for the various benefits of sleep for evolving knowledge. Consolidation of past experience encompasses a range of brain processes, driving integration of new information into established knowledge structures. Therein embedded lies the evolution of memories over time, which describes the extraction of superordinate conceptual or perceptual features from the informational richness of *fresh* memories. Such memory evolution is linked to sleep's benefits for recognition, insight, problem solving, and (smart) forgetting (Tononi & Cirelli, 2014; Stickgold & Walker, 2013; Verleger et al., 2013).

### 1.1. Mechanisms of Memory Acquisition and Consolidation

How do we acquire and consolidate new information? Donald Hebb's (1949) seminal work set the grounds for our modern definition of learning and memory. He proposed that learning activates ensembles of neurons that accommodate this new information by strengthening their shared synapses and so their ensemble-connectivity. Since then, long-term potentiation (LTP) was identified as the prime mechanism behind learning-dependent strengthening/enlargement of synapses. High neuromodulation during active wake facilitates this process by biasing plasticity towards potentiation (Genzel & Wixted, 2017; Lee & Dan, 2012; Seol et al., 2007).

As shown consistently in sleep deprivation studies, LTP does not suffice to form lasting memories. A lack of sleep not only impairs consolidation of previously learned information but also acquisition of novel memories (Dudai, Karni, & Born, 2015; Curcio, Ferrara, & De Gennaro, 2006). In particular, memory consolidation seems to depend on non-rapid eye movement or NREM sleep (stages N1-3), rich in synchronized neural oscillations:

cortical slow waves (0.5-4 Hz), thalamocortical sleep spindles (10-16 Hz), and hippocampal sharp wave ripples[1]. (140-200 Hz) (Langille, 2019; Miyamoto, Hirai, & Murayama, 2017).

Memory for highly novel, unfamiliar information, such as new procedures, sequences, or episodes, appears to depend on the replay of learning-associated activity, via interareal coupling of spindles and ripples. Yet, slow waves seem to act as an universal mechanism to consolidate perceptually acquired, cortically stored memory (Boutin & Doyon, 2020; Holz et al., 2013; Schmidt et al., 2006; Huber et al., 2004).

What is the universal link between slow waves and memory consolidation? While potentiation is crucial for learning, it becomes costly as it accumulates with time awake. Bigger synapses require more space, energy, cellular supplies, and saturate neural responses to novel input (Tononi and Cirelli, 2014). In other words, big, potentiated connections pose *homeostatic* pressure on involved neural ensembles and reduce learning capacities. As proposed in the well substantiated 'Synaptic Homeostasis Hypothesis' (SHY), one of sleep's fundamental functions is to release this homeostatic pressure while sampling information from prior experience (Tononi and Cirelli, 2014). That is where slow waves come into play.

The presumed mechanism by which slow waves benefit memory and restore homeostasis is *proportional downscaling* of neural connections during sleep (Tononi and Cirelli, 2014). As we fall asleep, neuromodulation quietens, decreasing neural firing and biasing plasticity towards depression or *shrinkage* of synapses (Seol et al., 2007; Marrosu et al., 1995). These neurobiological conditions alter Hebb's (1949) plasticity rule during sleep: as they travel across the cortex, alternations between intense firing and neural silence, characteristic for slow waves, are shown to preserve only the strongest, most active connections, amidst global shrinkage (Langille, 2019; González-Rueda et al., 2018; Stern, 2018; de Vivo et al., 2017; Nere et al., 2013). Doing so, slow waves mediate sleep's manifold benefits: they restore learning capacities, wipe away old, unused memories, and protect strong, highly used connections, as in regions where learning occurred or *established* neural structures (Tononi & Cirelli, 2014).

### 1.2. Theoretical Framework: Slow Wave Homeostasis and Memory

Largely based on analyses of individual slow waves, Bernardi et al. (2018) and Siclari et al. (2014) proposed two distinct synchronization mechanisms for slow wave activity during sleep: 1) an arousal-dependent, thalamocortical mechanism, whereby low levels of

[1] Ripples describe bursts of high-frequency firing (140-200 Hz, ~ 100 ms) of extensive ensembles of hippocampal neurons that reflect replay of activation patterns from prior experience (Genzel, & Wixted, 2017)

neuromodulation permit thalamic relay neurons to induce large, Type 1 slow waves, predominating fronto-central cortical areas; and 2) a homeostatic or experience-dependent, cortico-cortical mechanism, yielding small, Type 2 slow waves throughout the cortex.

In line with an arousal-dependent regulation, Type 1 slow waves occur early and remain stable throughout sleep, synchronizing extensive cortical populations via a global "reset" of brain activity. Importantly, such a global "reset" is pertinent to synchronize homeostatically regulated Type 2 slow waves. Bernardi et al. (2018) further associated the well-established link between sleep spindles and slow waves with the local occurrence of type 2 slow waves, in corroboration of learning-dependent increases in homeostatic pressure.

The synchronization mechanisms proposed by Bernardi et al. (2018) and Siclari et al. (2014) resonate well with conventional measures of slow wave activity during post-learning sleep. Huber et al. (2004) analysed slow wave power during NREM sleep, upon learning of visuospatial information. They localized power correlates of memory consolidation to parietal Brodmann areas 40, around the intraparietal sulcus. This finding is in line with increases in homeostatic slow wave generation in visual pathways upon learning-dependent potentiation and their link to memory consolidation. Importantly, these correlates were observed against the background of anterior predominance of slow wave power, reflecting a global "reset" of brain activity (Huber et al., 2004). Yet, spectral power can be mediated by either incidence or amplitude of slow waves, or a combination of both.

In fact, Bernardi et al. (2018) found profound amplitude differences ($M$ = 136.26 ± 32.8 μV vs. $M$ = 52.38 ± 12.46 μV) between Type 1 and Type 2 slow waves, during NREM sleep. Thus, and considering that slow waves occur as singular events, measures of slow wave power likely overrepresent large, Type 1 slow waves (Mensen, Riedner, & Tononi, 2016). 2016). Such overrepresentation of high-amplitude waves could account for the fronto-central predominance of slow wave power observed by Huber et al. (2004). Likewise, observed memory correlates at parietal sites agree with homeostatic increases in incidence of smaller, Type 2 slow waves (Bernardi et al., 2018).

Interestingly, Bernardi et al (2018) further performed spatial, principal component analyses (PCA) of slow wave activity (0.5-4 Hz) during NREM sleep periods. Whereas spectral powers can be easily skewed by very large and/or many waves, spatial PCA of a certain time interval informs about most consistent slow wave activity (Bernardi et al., 2018; Mensen et al., 2016). Their analyses yielded that, what is henceforth referred to as, "cortical involvement" of slow wave activity was reducible to few fronto-central, parieto-central, lateralized components. These components showed high consistency across their eleven

examined participants. Noteworthy, Bernardi et al. (2018) identified large, Type 1 slow waves primarily in the fronto-central component, explaining most of variance in the slow wave band ($M$ = 69.46%, $SD$ = 8.92%). Conversely, smaller, Type 2 slow waves were found across all main components.

### 1.3. Does Cortical Involvement of Slow Wave Activity reflect Memory Consolidation?

Bernardi et al. (2018) identified the component structure underlying cortical involvement of slow wave activity and the distribution of slow wave types therein during nocturnal NREM sleep. Importantly, they did so without administering any learning tasks prior to sleep onset. The consistency of their findings across all examined participants ($N$ = 11) is interesting for at least three reasons. First, predominance of large, Type 1 slow waves in the greatest, frontocentral component agrees well with their anterior synchronization from a few, thalamocortical projections (Bernardi et al., 2018; Siclari et al., 2014). Second, ubiquitous occurrence of small, Type 2 slow waves across all major components exemplifies increases in homeostatic pressure throughout the cortex, accumulated during normal or typical wake experience (Bernardi et al., 2018; Tononi & Cirelli, 2014; Huber et al., 2013).

Third, the work of Bernardi et al. (2018) left open the question whether learning prior to sleep alters the cortical involvement of slow wave activity during sleep. Indeed, it should increase homeostatic pressure in involved, cortical regions. Higher incidence of smaller, Type 2 slow waves over cortical areas in which learning had occurred should manifest as greater covariance of slow wave activity (0.5-4 Hz) in respective regions. Such a relation between slow wave incidence and covariance is due to the traveling behaviour of slow waves from their synchronization site (Bernardi et a., 2018; Mensen et al., 2016; Massimini et al., 2004): the more often and farther slow waves travel over the same cortical region during a certain period of time, the more the activity in the slow wave band should covary in respective EEG channels. That in turn motivated the question whether individual differences in cortical involvement of slow wave activity during sleep predict subsequent memory performance and so reflect memory consolidation.

To address this question, a high-density EEG dataset, made publicly available at the Open Science Framework (OSF) by and in agreement with Mei, Grossberg, Ng, Navarro, and Ellmore (2018), was utilized. The dataset contains EEG recordings from 20 participants of a 30-minute nap period after performing one of two versions (high/low load) of the subsequent memory paradigm, using real-life sceneries, and post-nap scene recognition scores. It was originally used to test machine learning algorithms for sleep spindle detection and participants

spend on average 85% of the nap in NREM sleep (stages N1-3) (Mei et al., 2018). The dataset was chosen because of its resemblance in polysomnographic features with the sleep episodes analysed by Bernardi et al. (2018), with the crucial distinction that scene learning took place prior to sleep.

Prior, comparable work linked visually acquired memory for spaces, scenes, face-scene associations, or rotation adaptation, consistently to posterior cortical areas, spanning from the postcentral gyrus and precuneus across the parietal cortices (Silson et al., 2019; van Assche et al., 2016; Bergmann et al., 2012; Hirshhorn et al., 2012; Huber et al., 2004). As shown by Huber et al. (2004) and Bergmann et al. (2012), consolidation of such memories depends on more comprehensive synchronization during sleep, permissive of learning-dependent/homeostatic events, such as Type 2 slow waves or spindles.

Adopted from Bernardi et al. (2018), spatial PCA of slow wave activity (0.5-4 Hz) was performed on whole nap recordings to examine the predictive value of individual differences in cortical involvement for scene recognition. Across individuals, emerging components of cortical involvement should be consistent and differ in explained variance to those obtained by Bernardi et al. (2018). Such sample differences should reflect learning-dependent increases in incidence of slow waves or changes in slow wave homeostasis in visual pathways linked to memory for scenes, places, etc. (Silson et al., 2019; Hirshhorn et al., 2012). Importantly, individual differences in variance explained especially by posterior components should reflect variation in slow wave homeostasis and thus consolidated scene memory across visual areas (Huber et al., 2004).

Complementary analyses excluded epiphenomenological origins of observed differences in cortical involvement and their relationship with scene recognition. Correlational analyses of average slow wave power with scene recognition were performed on the whole nap recording and on individual sleep stages (N1-3), including pre-nap wake. Based on comparable learning paradigms (Bergmann et al., 2012; Huber et al., 2004), correlates of scene recognition should emerge in parieto-central regions and overlap topographically with posterior components of cortical involvement. However, they should emerge only during sleep (stages N1-3) and not during pre-nap wake. Consequently, two predictions were made:

1.) Individual differences in cortical involvement of slow wave activity, specifically the variance explained by underlying, presumably parieto-central, components and their topographies should predict scene recognition.

2.) Average slow wave power in parieto-central areas should predict scene recognition across the whole nap period and during nap sleep (stages N1-3) but not pre-nap wake.

## 2. Methods

### 2.1. Participants

The total EEG dataset provided by Mei et al. (2018) included data from 20 participants (7 women), ranging between 18 and 42 years of age ($M$ = 23.15, $SD$ = 6.04). All data were acquired with written informed consent, in accordance with The Code of Ethics of the World Medical Association (Declaration of Helsinki), and approved by the Institutional Review Board of the City College of New York.

### 2.2. Procedure

The experimental sessions took place in a sound-attenuated booth (IAC acoustics) in order to prevent auditory and visual distractions (Mei et al., 2018). Each participant completed two sessions, each lasting about two hours, over the course of two days. Participants were instructed to go to sleep one and a half hours later than usual during the nights prior to the experiments to increase the probability of falling asleep during the nap periods. Each session began with either a high or low load version of the subsequent memory paradigm. Each trial comprised 1) an encoding period during which participants were presented with a continuous sequence of either 5 (high load) or 2 (low load) outdoor scenes, each presented for 2 seconds, 2) a delay period in which participants had to maintain the encoded scenes in memory for 6 seconds, 3) a probe period during which either a negative or positive probe was presented for 2 seconds. Here, participants indicated if they saw the shown probe during the previous encoding period by pressing either the right (green) or the left (red) button on a RB-530 response pad (Cedrus Inc) if the probe was recognized or not, respectively (Mei et al., 2018). Thereafter, a phase-scrambled scene was shown for 5 seconds marking the end of one trial. Negative/novel probes and positive/previously presented probes were equally distributed across trials. Participants performed 100 trials in the low and 40 trials in the high load condition respectively, yielding an equal number of stimuli in each condition (Mei et al., 2018). Figure 1 illustrates two low load trials, a negative and positive probe, respectively.

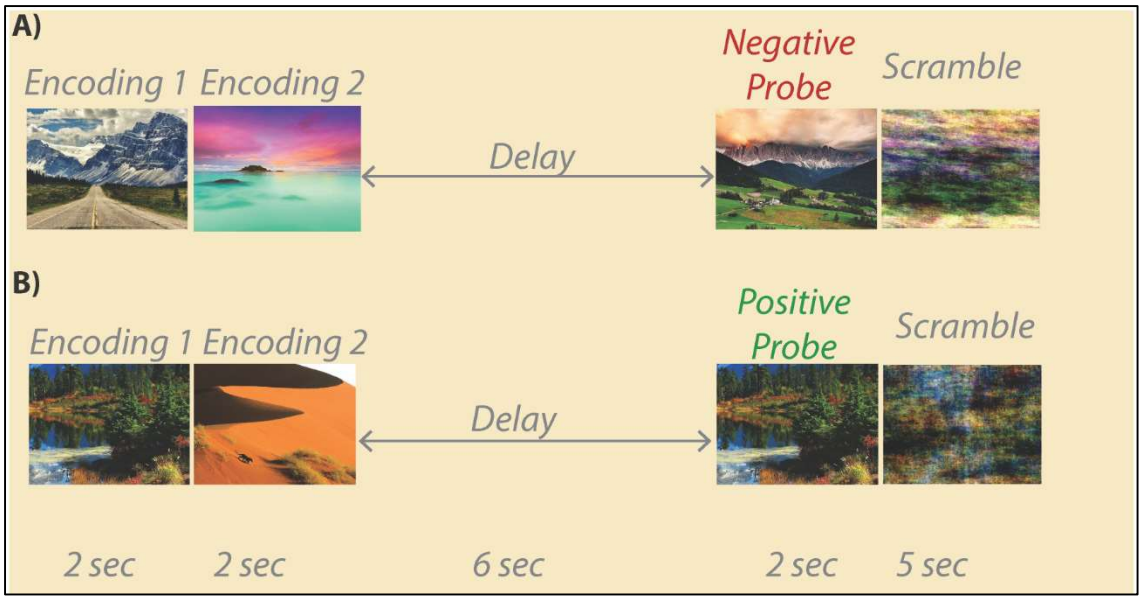


*Figure 1.* Example of the subsequent memory paradigm in the low load condition. Participants encode a continuous sequence of two scenes (2 sec each), followed by a delay period (6 sec). After the delay participants are shown a probe (2 sec), followed by a 5 sec scramble. Figure adapted from "Early and late components of EEG delay activity correlate differently with scene working memory performance" by Ellmore, T.M., Ng, K., and Reichert, C.P., 2017, *PLOS ONE 12*(10): doi:10.1371/journal.pone.0186072

Immediately hereafter, a scene recognition task was performed, using one half of the scenes presented in the subsequent memory task (125 images), followed by a 30-minute nap on a bed in a darkened, sound-isolated recording chamber. After the nap, a second scene recognition task was performed with the remaining half of scenes. In both recognition tasks already-presented scenes were blended with an equal number of new scenes. Again, scenes were presented for two seconds and after each scene participants indicated if they recognized the scene using either right or left button on the response pad (Mei et al., 2018).

### 2.3. Materials

A total of 250 scenes (24-bit colour images) was randomly selected from the SUN database (Xiao et al., 2010). To ascertain novelty of the presented stimuli and prevent any verbal rehearsal strategies based on scene details, scenes with clearly visible faces, people, or easily nameable objects were excluded. Using Superlab 5 (Cedrus Inc.) software, scenes were presented on a 27-inch LED monitor (resolution 1920x1080 pixels) with a refresh rate of 60 Hz. Scenes were sized to 800x600 pixels on the screen. Participants sat at 83.5 cm distance from the screen and maintained a stable view using a combined forehead/chin rest (Ellmore, Ng, & Reichert, 2017).

## 2.4. Apparatus and EEG recording

Scalp oscillatory activity during the napping period was recorded at a sampling rate of 1000 Hz with an active electrode system (actiCHamp, Brain Products GmbH) using 64 active Ag/AgCI electrodes, including two electrooculography (EOG) electrodes (LOC, ROC). Electrolytic gel was applied between the scalp and the electrodes tips in order to keep impedances below 25 kΩ. Electrodes were arranged in accordance with the standard 10-20 system, at positions: Fp1, F7, F3, F7, FT9, FC5, FC1, C3, T7, CP5, CP1, Pz, P3, P7, O1, Oz, O2, P4, P8, CP6, Cp2, Cz, C4, T8, FT10, FC6, FC2, F4, F8, Fp2, AF7, AF3, AFz, F1, F5, FT7, FC3, FCz, C1, C5, TP7, CP3, P1, P5, PO7, PO3, POz, PO4, PO8, P6, P2, CPz, CP4, TP8, C6, C2, FC4, FT8, F6, F2, LOC, ROC, with TP9 as reference and Fpz as ground electrodes (Jasper, 1958). Electrodes F7 and F8 were designated as horizontal EOG (HEOG) channels, electrodes LOC and ROC were placed above the right eye as vertical EOG (VEOG) channels (see Appendix A, Mei et al., 2018).

## 2.5. Data Analysis

### 2.5.1 Polysomnographic data

For all but two recordings pre-nap wake and individual sleep stage were derived from manual sleep annotations provided by Mei et al. (2018) on OSF. For the two remaining recordings (participants 30 and 32), sleep stages were identified with the EDF browser, by visual inspection of activity in relevant channels and by use of time/frequency analyses in accordance with the AASM criteria, on minimally pre-processed data (re-referenced, filtered, reduced sampling rate)(Iber, Ancoli-Israel, Chesson, & Quan, 2007). These included the spatiotemporal (co)occurrence of slow wave activity (0.5-4 Hz), Alpha activity (8-12 Hz), sleep spindles (10-16 Hz), and eye movements at respective electrodes.

### 2.5.2. Behavioural Data

Post-nap scene recognition scores for selected participants (see paragraph “Partition of the napping period”) were also obtained from the publicly accessible dataset by Mei et al. (2018) on OSF. Individual scores were represented as percentages of correct responses.

### 2.5.3. Preprocessing of EEG Data

Raw EEG nap recordings, provided by Mei et al. (2018) on OSF, were analysed with BrainVision Analyzer software (Brain Products GmbH; v2.0.2). First, all channels were re-referenced to the average of both mastoid electrodes (TP9, TP10). The sampling rate was

reduced to 200 Hz. Hereafter, data were bandpass filtered between 0.3-40 Hz using zero phase shift IIR Butterworth filters. A high-rank, high-pass filter at 0.3 Hz (roll-off rate: 160dB/decade) was applied. Doing so, the risk for inclusion of lower-frequency artifacts caused by slow body or eye movement or sweating was reduced. Such artifacts are known to affect frequencies below 0.5 Hz and cause problems for artifact rejection in independent component analyses (ICA) (Bernardi et al., 2018; Winkler et al., 2015; Zakeri et al., 2014).

Further, a rough, semiautomatic artifact rejection with a maximal allowed voltage increase of 50 μV per millisecond and maximal allowed voltage difference of 500 μV was performed. This was done to further improve the exclusion of low-frequency and high-amplitude artifacts while retaining large slow waves with amplitudes up to 200 Hz and fast synchronization dynamics (Bernardi et al., 2018). Next, data were segmented into epochs of 4 seconds and manually checked for bad channels or signal distortions. Lastly, semi-automatic ocular rejection ICA were performed on the whole recordings.

### 2.5.4. Spatial PCA of Slow Wave Activity

Dimension reduction analyses (spatial PCA) of slow wave activity (0.5-4 Hz) were performed with Analyzer software (Brain Products GmbH; v2.0.2). In preparation for spatial PCA, nap recordings were bandpass filtered again to contain only slow wave activity (high pass at 0.5 Hz, low pass at 4 Hz, zero phase shift IIR Butterworth). Based on the findings of Bernardi et al. (2018), slow wave activity should be reducible to a few fronto-central, parieto-central, and lateralized components. Following that assumption, electrodes that are most likely affected by eye movements (LOC, ROC, Fp1, Fp2, AF7, AF3, F7, F8) were excluded to reduce potential noise in covariances of slow wave activity. As consequence, 54 channels were left for component estimations.

Accordingly, spatial PCA on whole nap recordings were performed. These were based on covariance matrices of slow wave activity at 54 channels during the 30-minute nap interval and varimax rotation (max. 25 iterations). Components with loadings above 1 were extracted and the 2 largest components emergent in each participant were selected for further analyses.

### 2.5.5. Spectral Analyses

To obtain spectral powers, FFT (Fast Fourier Transformation, 50% overlap, Hanning) was applied to consecutive 4 sec segments, using BrainVision Analyzer software (Brain Products GmbH; v2.0.2). Using the parameters FFT yielded a frequency resolution of 0.195 Hz. Power in the slow wave band was defined by its limiting frequency bins 0.5 and 4 Hz.

2.5.6. Statistical Analyses

Descriptive and correlational analyses were performed with the Statistical Package for the Social Sciences (SPSS; v25) and BrainVision Analyzer software (Brain Products GmbH; v2.0.2). Prior to further analyses, the effect of task difficulty on post-nap recognition performance was examined with paired-sample *t*-tests with task load (high/low) as a factor. Recognition scores and total SWA powers were examined for outliers, using the exclusion criteria xi > Q3 + 1.5 * IQR or xi < Q1 - 1.5 * IQR (IQR = ' interquartile range'; Q1 and Q3 denote the first and third quartiles of rank-ordered values). Descriptive measures (average, standard deviation) of pre-nap wake and sleep stage (stages N1-3) durations were computed.

Next, 8 electrodes, spanning across the anterior-posterior axis, were selected (F3, F4, C3, C4, P3, P4, O1, O2) in accordance with slow wave propagation across the anterior-posterior axis of the brain (Bernardi et al., 2018, Siclari et al., 2014, Massimini et al., 2004). For each recording, slow wave powers at selected electrodes were averaged across each individual sleep stage (including pre-nap wake) as well as across the whole nap period.

Prior to the correlational analyses, paired t-tests were used to examines power differences at selected electrodes for pre-nap wake vs. N1 sleep and N1 sleep vs. N2-3 sleep. Hereafter, spectral power values for all selected electrodes were log-10 transformed. Finally, log-10 power values for the whole recording as well as individual sleep stages were correlated (Pearson) with post-nap scene recognition scores. Also, variances explained by selected components underlying cortical involvement of slow wave activity during the nap were correlated (Pearson) with scene recognition.

2.5.7. Permutation Test of Observed Memory Correlates

The robustness of observed correlations was examined in permutations of the whole sample. In each permutation ($N - 1$, $N$ = 'size of sample used for correlational analyses'), correlation coefficients were computed under exclusion of one datapoint that could greatly affect the linearity of the data. These so-called *influential* datapoints were identified on the basis of their position on the scatterplots of either explained variance or power on selected electrodes plotted against scene recognition scores. A datapoint was considered influential in a scatterplot if it was father away from a linear fitting line that any other point. Each further influential datapoint was identified as the one farther away from a linear fitting line that any other point after exclusion of the previous one.

In such an iterative way 6 datapoints were selected from scatterplots of explained variance against scene recognition for analysed components of cortical involvement of slow

wave activity. In scatterplots of slow wave power against scene recognition, datapoints consistently identified as influential in all analysed electrodes (F3, F4, C3, C4, P3, P4, O1, O2) were selected. These selected datapoints were then individually excluded from the whole sample ($N$ - 1) to yield sample permutations for variance and power correlates of scene recognition, respectively. The chosen number of 6 sample permutations per correlational model (variance or power) was based simply on the number identified influential points.

To determine significance of observed correlations Benjamini–Hochberg correction was applied to all sample permutations of a given correlate. In other words, variance correlates were significant if they survived Benjamini–Hochberg correction for all sample permutations. Likewise, single-electrode correlations reached significance only if they survived Benjamini–Hochberg correction in all sample permutations.

In each correlational model, correlation coefficients yielded by each sample permutation were arranged from smallest to largest, each value received the respective rank i (1 = smallest value, 6 = biggest value). As recommended by Lee and Lee (2018) for explorative work, the false positive rate (FPR) was set to .1, corresponding to a risk for one false positive per 10 cases. Such a methodology was meant to balance specificity (multiple sample permutations to test robustness of correlations) and sensitivity (less-conservative type I error correction). The Benjamini–Hochberg-corrected significance threshold for each sample permutation was calculated as $p < (i / 6) \cdot FPR$. In this way, the following significance thresholds were computed for lowest to highest ranked correlation coefficients: .017, .033, .05, .063, .083, 0.1 (Lee & Lee, 2018).

## 3. Results

Based on visual inspection, ICA, and sleep scorings, the complete recordings of participant 26 and 27 were excluded from analyses because the data were too noisy, or the participant did not fall asleep. Also, one outlier (day 1 of participant 21) based on recognition scores was removed from further analyses. Further, sleep stages N2 and N3 were summarized in the following analyses as not all participants reached N3 sleep during the napping period (see section 3.5).

### 3.1 Behavioural Data

No significant effects of task load on post-nap recognition score were found ($t(18) = .84$, $p = .3$). Based on non-significance of task load and the equal number of presented scenes in either load condition, task load was omitted in further analyses in favour of statistical power. Thus,

the final dataset used for further analyses comprised day 1 of participants 13, 17, 19, 20, 23, 28, 29 and day 2 of participants 11, 12, 14, 15, 16, 18, 21, 22, 25, 30, 32 ($N$ = 18). Participants recognized between 58% and 81% of positive probes shown after the nap ($M$ = 72.2% , $SD$ = 6.73%). The distribution of recognition scores roughly resembled a normal distribution with most scores ($n$ = 9) ranging between 70-74 percent (see figure 2).

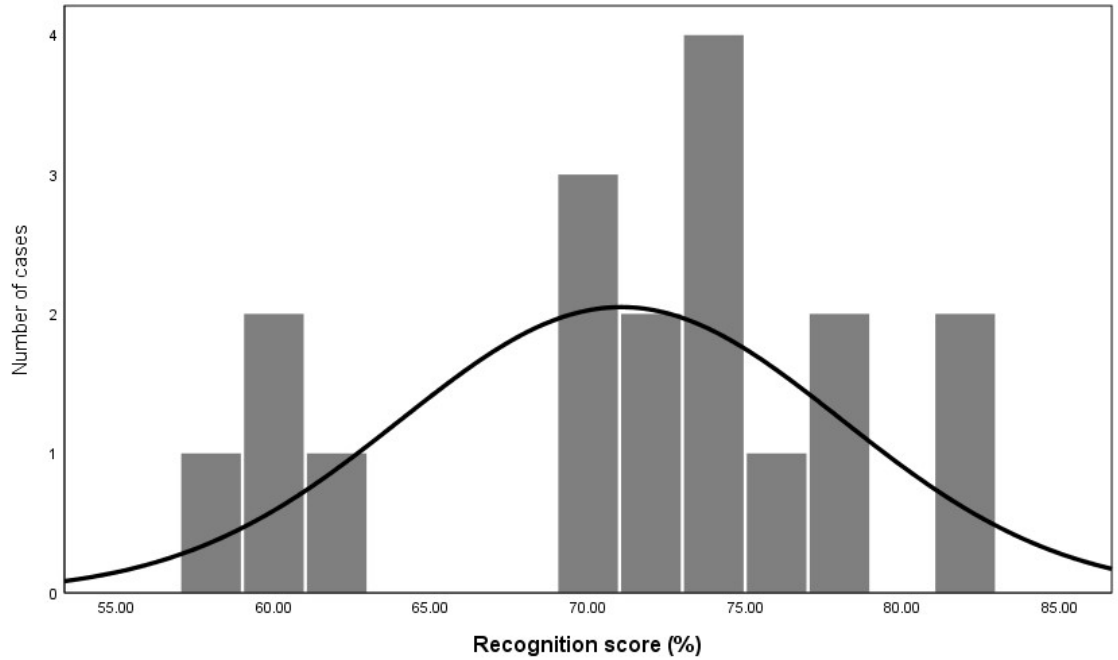


*Figure 2.* Distribution of recognition scores roughly resembles a normal distribution, with most scores cumulating around the mean ($M$ = 72.2 %).

### 3.2. Polysomnographic Features of the Nap Period

On average participants fell asleep after ~ 5 minutes upon recording onset in the sleep lab and spend most of their time in sleep stages N2-3, upon entering N1 sleep for about 6 minutes (see table 1). As illustrated in figure 3, disruption of continuous activity in the alpha band (~10 Hz) and increases in slow wave (<4 Hz) and spindle activity (~15 Hz) early in the recording marked sleep onset.

*Table 1*. Polysomnographic parameters

| **Sleep parameter** | ***M* (*SD*)** | **% of total nap time** |
|---|---|---|
| pre-nap wake | 292.61 sec (108.4 sec) | 16.5 |
| Total sleep time | 1480.67 sec (107.63) | 83.5 |
| Sleep stage N1 | 387.22 sec (175.28 sec) | 21.8 |
| Sleep stages N2-3 | 1093.44 sec (228.29 sec) | 61.7 |

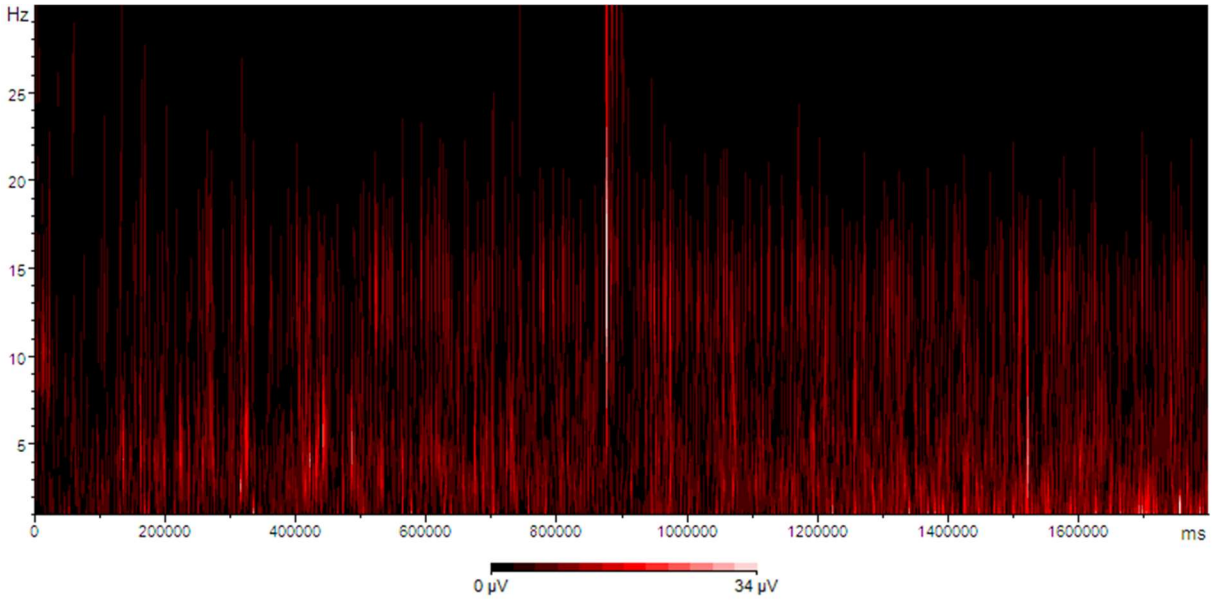


*Figure 3.* Time-frequency distribution of activity at electrode C3 across the nap period.

### 3.3. Power Differences across the Nap Period

Slow wave power, averaged across all selected electrodes, did not differ significantly between pre-nap wake and sleep stage N1, yet showing great differences between sleep stages N1 and N2-3 ($M = 1.32$ µV², $SD = .44$ µV² vs. $M = 2.94$ µV², $SD = 1.2$ µV², $t(17) = 6.2$, $p < .001$). Average slow wave power showed a clear peak over frontal electrodes (F3, F4) during pre-nap. Although no single-electrode comparison between pre-nap wake and sleep stage N1 reached significance, the data suggest a spread or dispersion from one clear focus during pre-nap wake (dark areas in figure 4, left graph) along the anterior-posterior axis (light areas in figure 4, left graph). In contrast, single-electrode comparisons between sleep stage N1 and N2-3 were highly significant ($p < .001$). Noteworthy, the greatest increases in slow wave power were observed for electrodes P3 ($t(17) = 6.76$, $p < .001$), C4 ($t(17) = 5.72$, p = $p < .001$), C3 ($t(17) = 5.62$, p = $p < .001$), and O2 ($t(17) = 6.29$, $p < .001$).

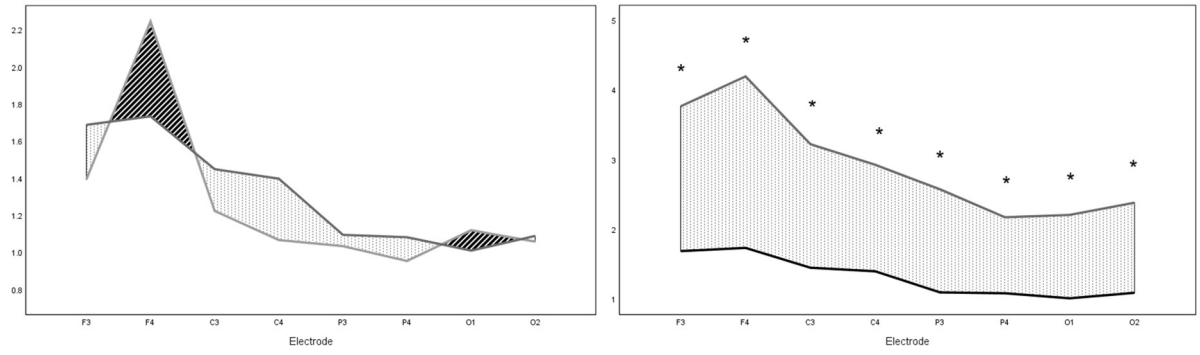

*Figure 4.* Differences in slow wave power across the anterior-posterior axis (order of electrodes: F3, F4, C3, C4, P3, P4, O1, O2. Powers are indicated in $\mu V^2$ (left: 0-2.2 $\mu V^2$; right 0-5 $\mu V^2$). The left graph shows power differences between pre-nap wake and sleep stage one: dark areas (pre-nap wake > sleep stage N1), light areas (pre-nap wake < sleep stage N1). The right graph shows power differences between sleep stages N1 and N2-3: light areas (stage N2-3 > stage N1). Significant power differences are marked with a star (paired *t*-test).

### 3.4. Effects of Cortical Involvement of Slow Wave Activity on Scene Recognition

In all recordings but those of participants 13 and 30, cortical involvement of slow wave activity (0.5-4 Hz) was reducible to three or four main components, together explaining more than 92.72% (*SD* = 4.16%) of variance: a parieto-central component with largest cortical involvement that extends over central, parietal, temporal, and occipital areas, explaining 64.68% variance on average (*SD* = 14.52%), another fronto-central component with great cortical involvement spreading towards frontal, central and to a lesser extent temporal areas, explaining 20.4% variance on average (*SD* = 7.04%), and a small, lateralized components, explaining 3.26% (*SD* = 1.64%) respectively (for a small summary of PCA components for the first 4 recordings see Appendix D). Figure 5 illustrates above reported component structure underlying the cortical involvement of slow wave activity, throughout the nap, with single participant data. The finding of most variance in slow wave activity being explained by a parieto-central component clearly contrasts the above observed frontal predominance of average slow wave power across the nap. (see figure 4). Overall, low variation in cumulative variance explained by the main components resonated with the highly uniform component structure found in all but two participants. Interestingly, variation in the largest, parieto-central component was twice as high as in the second-largest, fronto-central component.

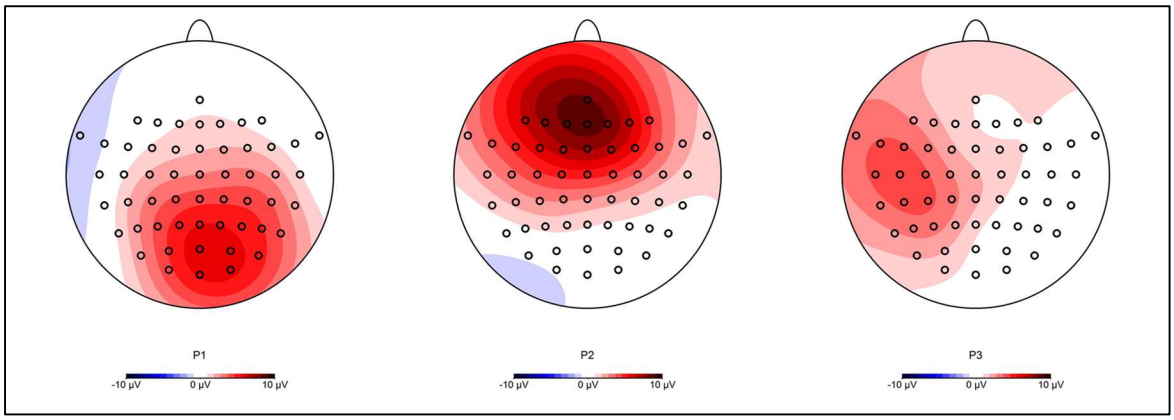


*Figure 5*. Cortical involvement of slow wave activity (0.5-4 Hz) throughout the nap period can be reduced to three or four principal components cumulatively explaining more than 92.72% of variance: Two large parieto-central and fronto-central components and less pronounced, lateralized components (illustrated with single-participant data).

Recordings of participants 13 and 30 showed a markedly different cortical involvement of slow wave activity. Both recordings showed much less pronounced and unified parieto-central components, against the background of most variance being explained by fronto-central components. Such weak cortical involvement of slow wave activity in parieto-central regions coincided with low recognition scores for participants 13 and 30 (60% and 58%).

Further, based on inspection of their potential to influence linearity in the data, the following participants were selected for permutation tests (see section 2.5.7.). Participants 12, 13, 18, 25, and 32 were selected to test the robustness (Benjamini–Hochberg correction) variance correlates of scene recognition for parieto-central components of slow wave activity. Participants 12, 13, 18, 25, and 28, were selected to test the robustness (Benjamini–Hochberg correction) variance correlates of scene recognition for fronto-central components of slow wave activity (see Appendix C).

3.4.1. Parieto-central Involvement of Slow Wave Activity and Scene Recognition

Almost 2/3 of variance observed in slow wave activity (0.5-4 Hz) throughout the nap were explained by the largest, parieto-central component ($M$ = 64.68%, $SD$ = 14.52%). This prime focus was not only characterized by extensive cortical involvement over posterior regions but also great spread along the anterior-posterior axis and laterally. Importantly, the amount of variance explained by the parieto-central component showed highly stable correlations with scene recognition in all sample permutations and survived Benjamini–Hochberg correction ($r(18) = .42$, $p = .043$; overall highest $p = .059$)(see figure 6).

Individual topographies of parieto-central components further supported these robust variance correlates. Less pronounced involvement of parieto-central regions coincided with lower scene recognition scores and vice versa. In particular, weak posterior components and very low scene recognition scores for participants 13 and 30 further corroborated the observed memory correlates of parieto-central involvement of slow wave activity (see figure 7, data of participant 13 included).

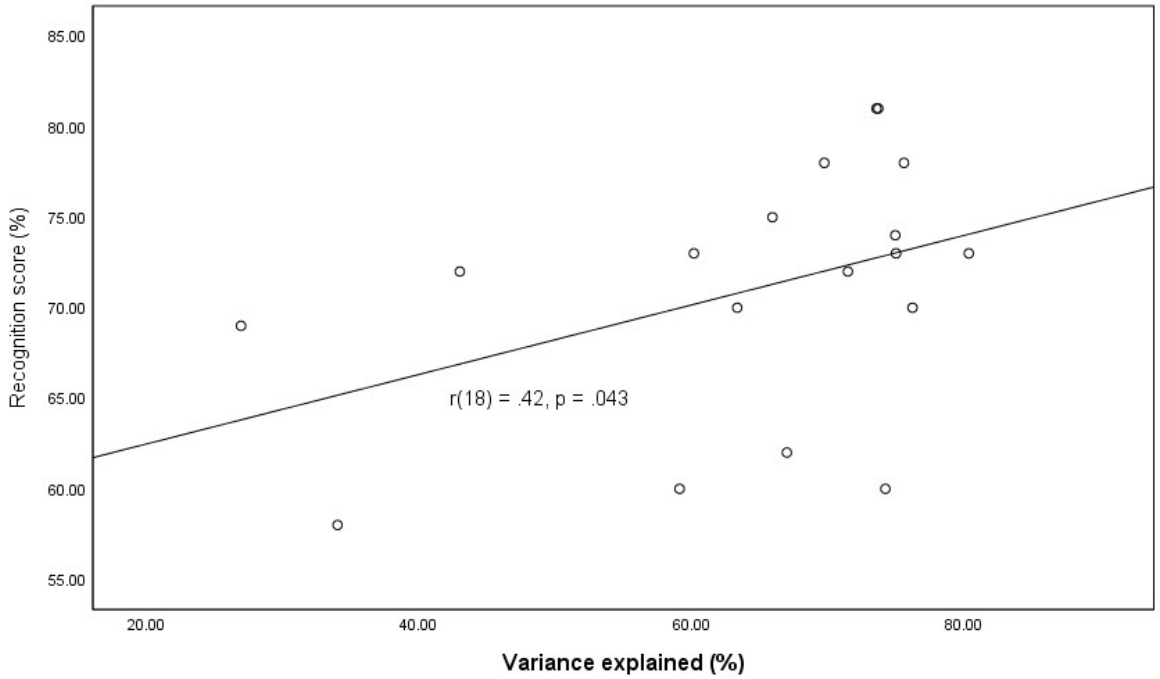


*Figure 6.* Correlations of variance explained by the prime, postero-central component, with scene recognition.

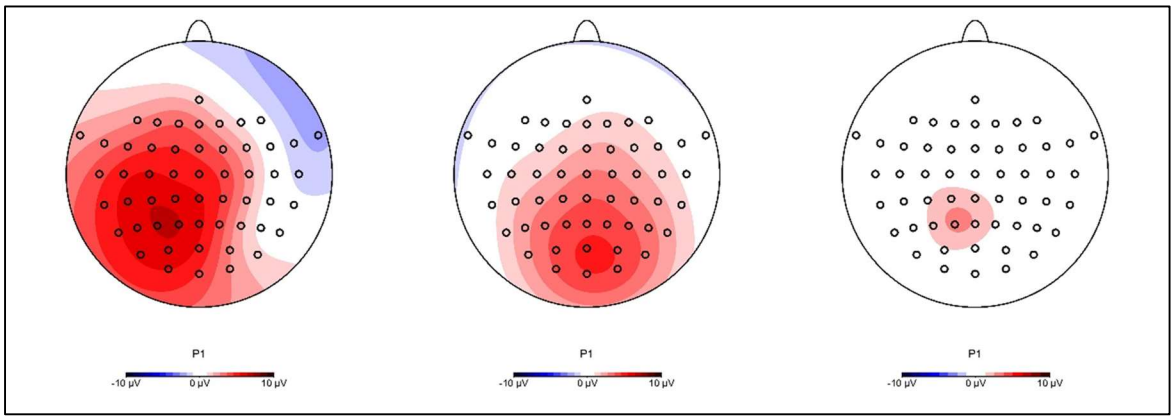


*Figure 7.* Topographical maps of postero-central involvement of slow wave activity (0-10 $\mu V^2$) throughout the whole nap. Individual cases are presented in descending order of scene recognition scores (left-to-right): 81% recognized, 70% recognized, 60% recognized.

### 3.4.2. Fronto-central Involvement of Slow Wave Activity and Scene Recognition

The second-largest, fronto-central component showed a larger covariance/involvement peak than the prime, parieto-central component, corresponding to anterior predominance in slow wave power across the nap. Yet on average, it explained only a fifth of overall variance in slow wave activity ($M$ = 20.4%, $SD$ = 7.04%). The above-mentioned lack of strong parieto-central involvement of slow wave activity in the recording of participant 30 yielded a fronto-central, primary component, explaining most of the variance (60.17%). Such deviant component structure not only resonated with a low recognition score (58%) but also skewed the linear relation between variance explained by the fronto-central component and scene

recognition (see Appendix C). Correlates of sample permutations corroborated that exclusion of participant 30 yielded a good correlation ($r(17) = .5$, $p = .021$) with scene recognition. However, no model survived Benjamini–Hochberg correction, in fact inclusion of day 2 of participant 30 distorted any linear relationship to coefficients well above .1. Topographical maps of fronto-central components (excluding participant 30) corroborated a proportional relation between cortical involvement of slow wave activity in fronto-central areas and scene recognition: low fronto-central involvement of slow wave activity predicted low scene recognition scores and vice versa (see Figure 8).

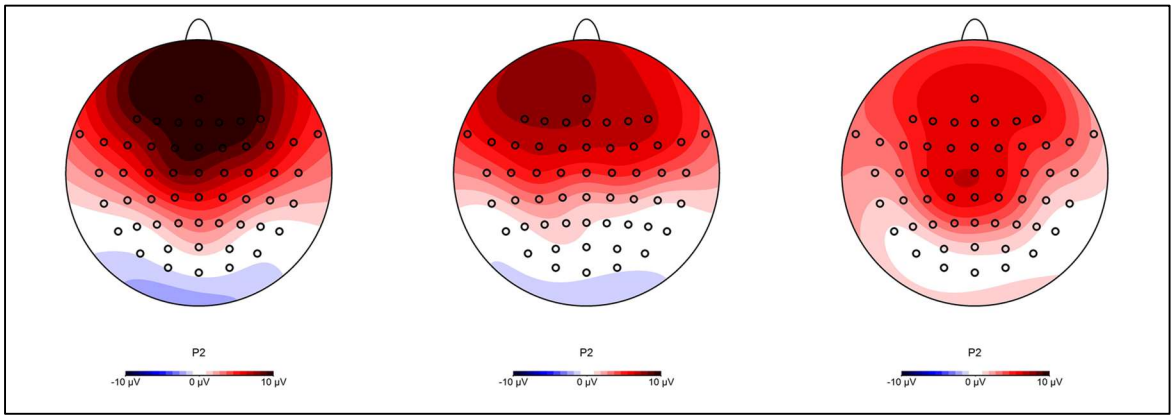


*Figure 8*. Topographical maps of fronto-central involvement of slow wave activity (0-10 $\mu V^2$) averaged across the whole nap. Individual cases are presented in descending order of scene recognition scores (left-to-right): 81% recognized, 70% recognized, 60% recognized.

### 3.5. Slow wave Power and Scene Recognition

Based on inspection of their potential to greatly influence linearity in the data (see section 2.5.7.), participants 11, 12, 14, 18, 25, and 30 were selected to test the robustness of observed slow wave power correlates of scene recognition (see Appendix C).

#### 3.5.1. Total nap and Scene Recognition Scores

Power in the slow wave band (0.5-4 Hz), averaged across the whole nap period, correlated with post-nap scene recognition. Effects of slow wave power were strongest and survived permutations tests with Benjamini–Hochberg correction for electrodes C3 ($r(18) = .514$, $p = .015$), C4 ($r(18) = .445$, $p = .032$) P3 ($r(18) = .429$, $p = .039$), and F3 ($r(18) = .406$, $p = .047$)(see figure 9). Among these effects, only frontal and central foci were reflected in individual topographies of slow wave power across the nap. Although slow wave activity occurred widespread along the anterior-posterior axis in all participants, low scorers showed notably less magnitude and spread from fronto-central foci to posterior areas (see figure 10).

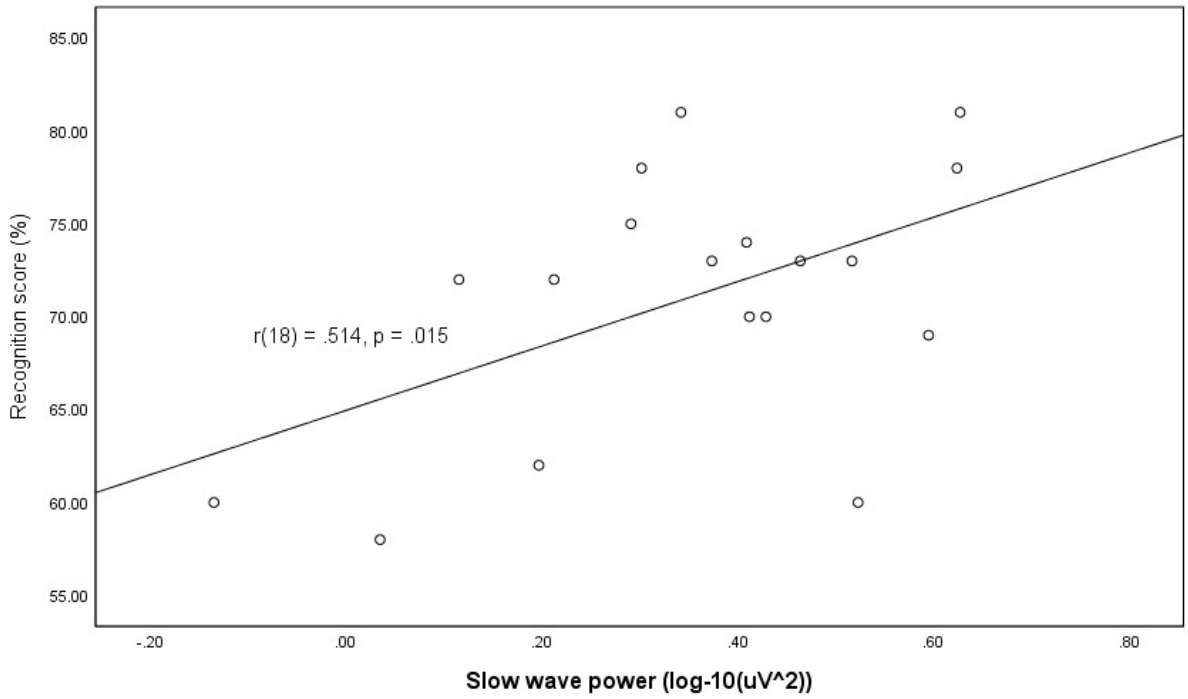


*Figure 9*. Correlations of central (C3) slow wave power averaged across the whole nap with scene recognition.

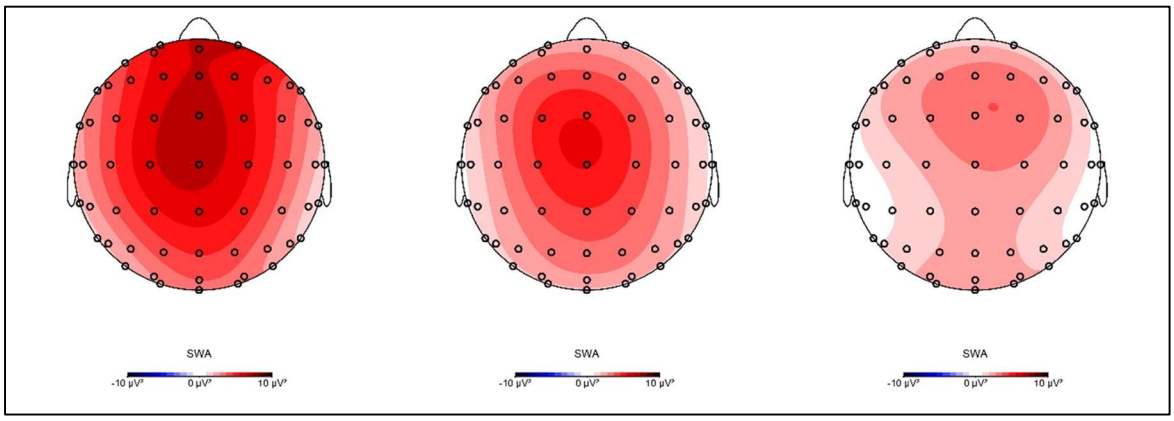


*Figure 10*. Topographical maps of slow wave power (0-10 $\mu V^2$) averaged across the whole nap period. Single cases are presented in descending order of scene recognition scores (left-to-right): 81% recognized, 70% recognized, 58% recognized.

### 3.5.2. Pre-nap Wake and Scene Recognition Scores

During pre-nap wake, correlations of slow wave power with scene recognition did not survive permutations tests with Benjamini–Hochberg correction at any selected electrode (see section 2.5.7.). Neither did individual differences in topographies of behave proportionally to scene recognition scores. In fact, average powers and topographies across pre-nap wake differed markedly from their sleep counterparts within some participants. Noteworthy, average slow wave power during pre-nap wake showed a more frontal predominance when compared to the larger spread in posterior direction observed in the total average (see figure 11).

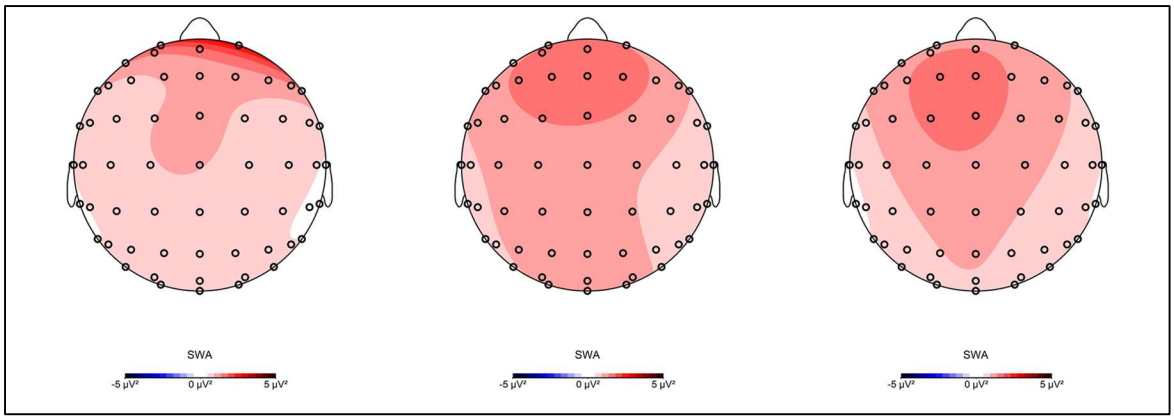


*Figure 11*. Topographical maps of slow wave power (0-5 $\mu V^2$) averaged across individual pre-nap wake periods. Single cases are presented in descending order of scene recognition scores (left-to-right): 81% recognized, 70% recognized, 58% recognized.

### 3.5.3. N1 Sleep and Scene Recognition Scores

Across initial sleep (stage N1) , average slow wave power emerged as correlate of post-nap scene recognition. Permutations tests with Benjamini–Hochberg correction yielded significant correlations for electrodes P3 ($r(18) = .546$, $p = .01$), C3 ($r(18) = .54$, $p = .01$), and O1 ($r(18) = .43$, $p = .038$) (see figure 12). Average power in the slow wave band did not increase significantly across initial sleep (stage N1) when compared to pre-nap wake. Yet, slow wave activity showed extended spread from frontocentral to parietal and occipital regions (see figure 4). Such progressive spread across the cortex corresponded well with the corrected memory correlates found at central, parietal, and occipital sites. Individuals scoring high on post-nap scene recognition showed greater slow wave spread and magnitude thereof from frontocentral foci to posterior regions, and vice versa for low scorers (see figure 13).

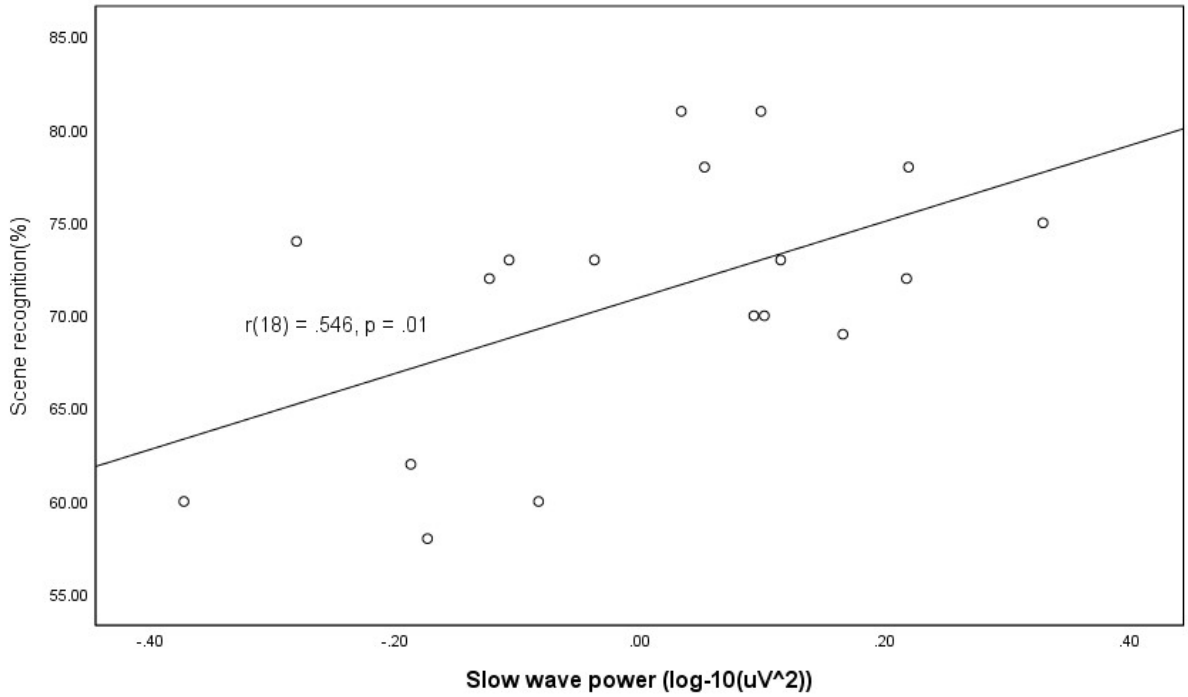


*Figure 12*. Correlations of parietal (P3) slow wave power averaged across N1 sleep with scene recognition.

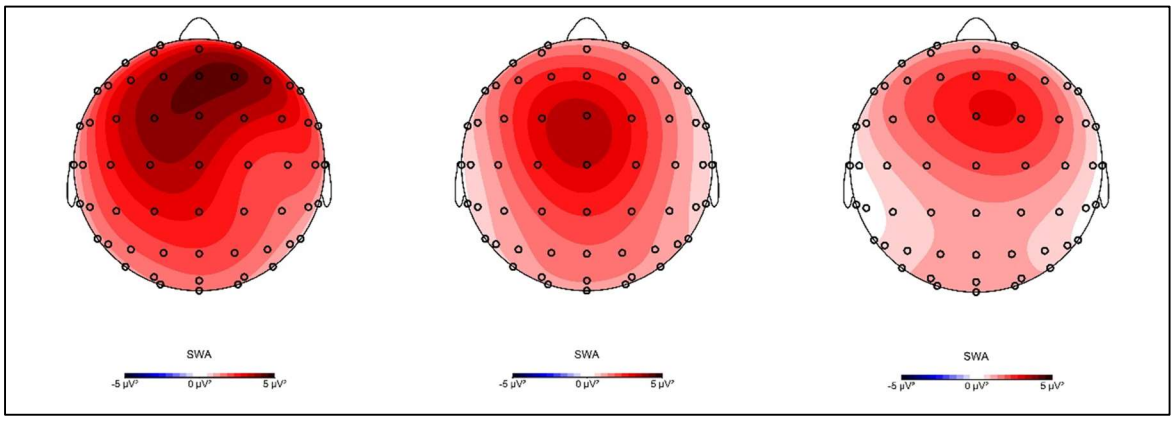


*Figure 13*. Topographical maps of slow wave power (0-5 $\mu V^2$) averaged across individual N1 sleep periods. Single cases are presented in descending order of scene recognition scores (left-to-right): 78% recognized, 70% recognized, 58% recognized.

### 3.5.4. N2-3 Sleep and Scene Recognition Scores

As expected, slow wave power increased greatly and globally across participants upon entry into sleep stage(s) N2-3 (see figure 2). As sleep stages N2-3 together constituted the major part of the napping period, memory correlates of slow wave power strongly resembled the total average reported above: Permutations tests with Benjamini–Hochberg correction yielded significant correlations at electrodes C3 ($r(18) = .494$ $p = .019$), C4 ($r(18) = .442$ $p = .033$), and F3 ($r(18) = .41$ $p = .045$) (see figure 14). Also correlates at recording site P3 showed robust correlations across all permutations and survived Benjamini–Hochberg correlations for all but the first ranked correlation by a mere factor of .0001 and were thus classified as

significant. In line with power correlates at frontal, central, and parietal sites, individual slow wave power topographies showed proportional relations with scene recognition: high scorers showed considerably greater magnitude and more comprehensive spread of slow wave activity across the cortex when compared to low scorers (see Figure 15).

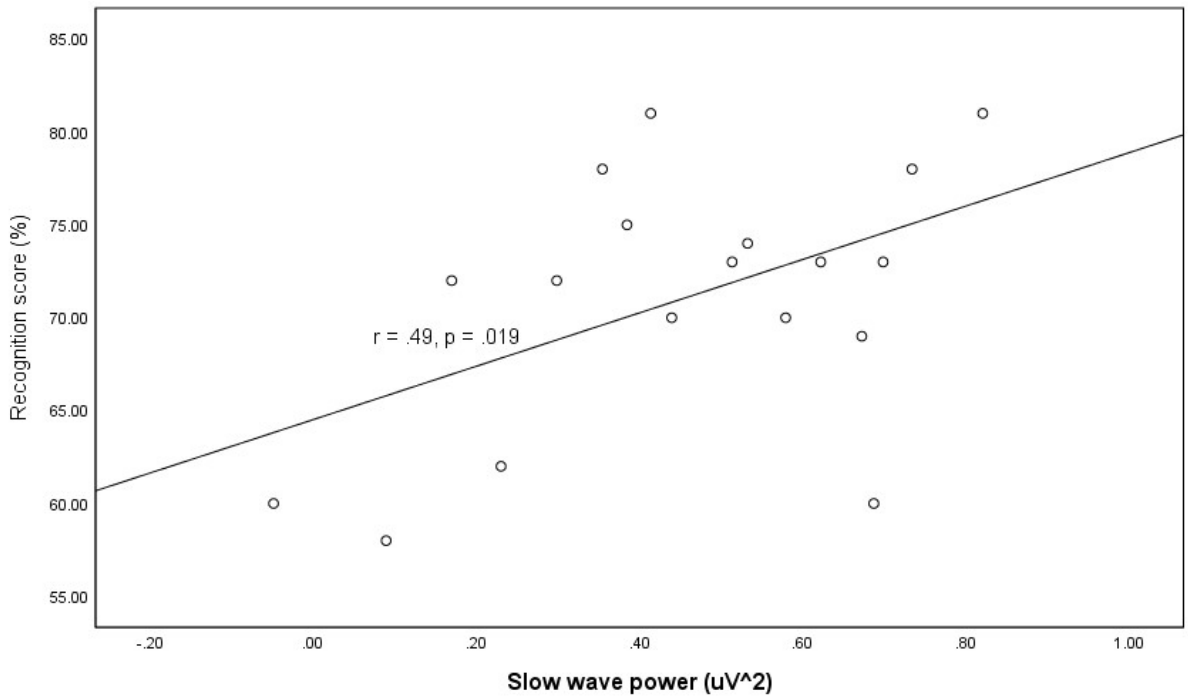


*Figure 14*. Correlations of central (C3) slow wave power averaged across N2-3 sleep with scene recognition.

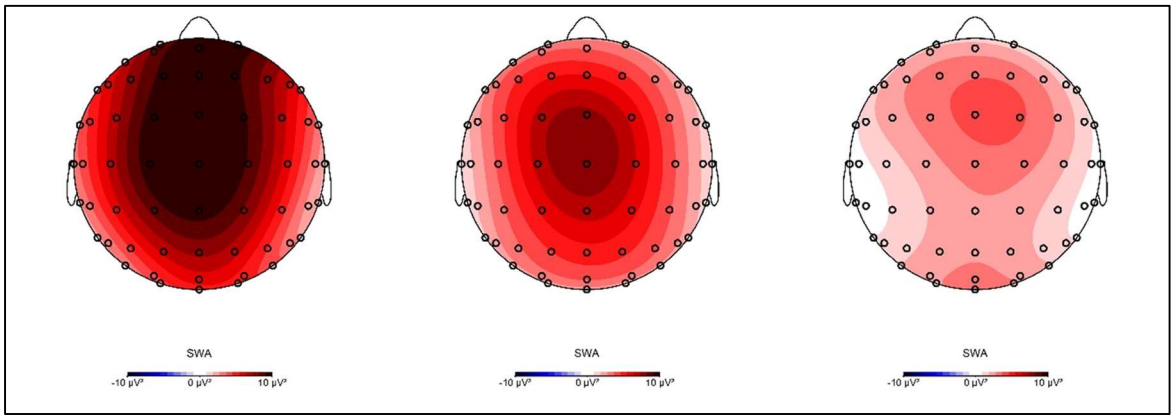


*Figure 15*. Topographical maps of slow wave power (0-10 $\mu V^2$) averaged across individual N2-3 sleep periods. Single cases are presented in descending order of scene recognition scores (left-to-right): 81% recognized, 70% recognized, 58% recognized.

## 4. Discussion

The present study examined whether individual differences in cortical involvement of slow wave activity during a nap predict subsequent recognition of real-life sceneries. In addition, the effects of slow wave power on scene recognition were examined for each sleep stage

(including pre-nap wake) as well as for the whole nap period. Cortical involvement of slow wave activity throughout the nap was reducible to a few main components, which emerged consistently in most participants. Of these, a prime, parieto-central component accounted for the majority of cortical involvement, followed by smaller fronto-central and lateralized components. The consistency of the observed component structure across participants agreed with small differences in variance explained in all but the largest, parieto-central component. Importantly, individual differences were not only considerably bigger for parieto-central involvement of slow wave activity, they also strongly predicted scene recognition.

These parieto-central variance correlates of scene recognition further overlapped topographically with power correlates found in the whole nap and specific sleep stages. Against the background of anterior power predominance, power correlates emerged at fronto-parieto-central sites across the whole nap period. During single sleep stages, most robust correlates were found at parietal and central sites, whereas frontal correlates were found only during deeper NREM sleep (stages N2-3), as slow wave power increased on average. In contrast, no power correlates emerged during pre-nap wake, where individual topographies showed slow wave power rather restricted to frontal regions. Altogether, these observations led to acceptance of both predictions.

### 4.1 Slow Wave Homeostasis and Consolidation of Scene Memory

In resemblance to the findings of Bernardi et al. (2018), a few, fronto-central, parieto-central, and lateralized components accounted for virtually all variance in slow wave activity throughout the nap. Yet, the variances explained by respective components differed crucially to those reported by Bernardi et al. (2018), where no learning occurred prior to sleep: cortical involvement of slow wave activity was majorly accounted for by a parieto-central and not fronto-central component.

The magnitude of these group-level differences resonates with homeostatically increased involvement of slow wave activity in visual areas linked to scene memory (Silson et al., 2019; Bernardi et al., 2018; Hirshhorn et al., 2012). More importantly, individual differences in parieto-central involvement of slow wave activity predicted scene recognition. That links consolidation of scene memory mainly to incidence and traveling of slow waves in parieto-central, visual pathways, considering lower slow wave power observed in posterior regions (Silson et al., 2019; van Assche et al., 2016).

The topographical congruence of memory correlates found in both involvement and power of slow wave activity in parieto-central areas is also in good agreement with prior

literature. Slow wave power correlates of visuospatial memory, localized by Huber et al. (2004) to parietal areas around the intraparietal sulcus (IPS), resonate highly with robust correlations at parietal sites. Likewise, highly robust memory correlates at central derivations agree well with dependence of visually acquired spatial or scene memory upon activity in the postcentral gyrus and precuneus (Hirshhorn et al., 2012).

Ultimately, memory correlates of parieto-central involvement of slow wave activity agree with the proportional downscaling model proposed by SHY (Tononi & Cirelli, 2014). Learning prior to the nap should have increased homeostatic pressure in visual areas linked to scene memory. The more and farther slow waves travel over these areas during the nap, the more homeostatic pressure is released, while salient connections, such as *fresh* scene memories, are preserved and integrated into established networks (Silson et al., 2019; González-Rueda et al., 2018; Stern, 2018; van Assche et al., 2016; Hirshhorn et al., 2012). In that way, only circumscribed parieto-central involvement of slow wave activity in participants 13 and 30 explains their low recognition scores, as it reflects less extensive consolidation of scene memory during the nap (Tononi & Cirelli, 2014).

### 4.2. A Link between Power and Cortical Involvement of Slow Wave Activity

Derived from individual slow wave analyses, the dualistic slow wave synchronization model, by Bernardi et al. (2018) and Siclari et al. (2014), matches observations made here along broader measures of cortical involvement and power. Cortical involvement mainly reflects incidence and traveling behaviour of slow waves throughout a cortical region, in a given time period (see section 1.3.). In contrast, measures of slow wave power are rather driven by both amplitude and incidence of slow waves (see section 1.2.).

Together, high power but lower involvement of slow wave activity in fronto-central regions suggest prevalence of large-amplitude but less numerous, slow waves. That agrees with the fronto-central prevalence of Type 1 slow waves observed by Bernardi et al. (2018). In turn, lower power but higher involvement of slow wave activity in parieto-central or posterior regions suggest prevalence of small but more abundant slow waves. That is in line with ubiquitous occurrence of Type 2 slow waves and their learning-dependent/homeostatic increases in visual areas. (Bernardi et al., 2018; Assche et al., 2016; Hirshhorn et al., 2012).

Such a delineation of slow wave types with respect to cortical involvement and power agrees well with the observations made here. Prior to sleep onset, frontal predominance of slow wave power and absent memory correlates agree with arousal-dependent fluctuations in synchronization, affected by default-mode-network activity (Siclari et al., 2014; Sämann et

al., 2011). During sleep, widespread, fronto-central predominance of slow wave power and correlations thereof with scene recognition during deeper sleep stages (N2-3) agree with low arousal tone and a more comprehensive "reset" in brain activity (Bernardi et al., 2018).

Fronto-central power predominance clearly contrasted the majorly parieto-central involvement of slow wave activity. That implies that parieto-central memory correlates in both measures mainly reflected individual differences in incidence and traveling of small-amplitude, Type 2 slow waves. Noteworthy, parieto-central memory correlates of slow wave power were present during nap sleep but not wake. That further agrees with homeostatic regulation of Type 2 slow waves and their dependence upon low arousal and a comprehensive "reset" of brain activity during NREM sleep (Bernardi et al, 2018). In corroboration, Mascetti et al. (2013) also found that slow wave incidence in posterior areas during nocturnal NREM sleep predicted overnight improvement in visual, perceptual learning. Altogether, measures of cortical involvement and power clearly outline a link between consolidation of scene memory and parieto-central or posterior incidence of smaller, Type 2 slow waves during NREM sleep.

### 4.3. Consolidation or Evolution of Memory during Sleep?

The observed importance of parieto-central parts of the cortex for scene recognition may be further considered with respect to evolution of new memories, as they become consolidated during sleep. Reviewing a considerable number of studies, Robin and Moscovitch (2017) highlighted the dynamic and flexible evolution of memories over time. Majorly based on fMRI, they identified a functional differentiation along the cortical anterior-posterior axis: anterior areas, such as the medial prefrontal cortex (mPFC) mediate retrieval of conceptual, higher-order information, while retrieval of perceptual details recruits posterior regions, such as the precuneus or IPS (Robin, & Moscovitch, 2017).

Critically, Robin, and Moscovitch (2017) argue that these evolution trajectories depend on the scale of detail and nature of a given task. Robust memory correlates of slow wave activity in parietal and central regions linked to visual processing agree with the use of perceptually rich, real-life sceneries in the present study. In contrast, tasks that require the extraction of superordinate information from given stimuli should engage anterior cortical regions during sleep or specifically NREM sleep. Verleger et al. (2013) examined sleep-dependent processing of information acquired during the number reduction task (NRT).

Conceptionally, the NRT contrasts the subsequent memory paradigm employed here. It does not rely on retention of perceptual details to guide subsequent recognition but on insight into higher-order regularities in processed stimuli. In line with a comprehensive

synchronization permissive of homeostatic oscillatory events such Type 2 slow waves or spindles (Bernardi et al. 2018), insight in the NRT relied upon NREM, or specifically N3, sleep. Although no effects were found in the slow wave band, overnight insight was associated with increased power in the alpha or slow sleep spindle band (10-12 Hz) at central electrodes (Verleger et al., 2013).

As demonstrated here, measures of slow wave power alone may be too broad to capture learning-dependent changes in slow wave homeostasis, especially if averaged over hours of sleep. Such insensitivity may be particularly high in fronto-central regions, where arousal-dependent, high-amplitude slow waves prevail. Yet, the observed link between slow spindle activity at central electrodes and overnight insight in the NRT is in line with task-dependence of memory evolution (Robin, & Moscovitch, 2017). Indeed, observed slow spindle powers at central sites correspond roughly to their usually anterior predominance (Cox et al., 2017). Spindles mediate replay of learning-associated activity patterns during sleep. Thus, their presumably anterior occurrence agrees with sleep-dependent extraction of higher-order regularities from prior practice with the NRT (Robin, & Moscovitch, 2017)

### 4.4. Limitations

Somewhat ironically, a confounding factor in the present study might have been a disturbance in above discussed slow wave homeostasis. Each participant performed the experiments over two consecutive days. However, the slight sleep deprivation prior to each experiment due to instructed delay (2 hours) in sleep onset, might have conceivably affected homeostatic slow wave synchronization during the nap. Cumulative potentiation in motor and sensory areas from prolonged wakefulness, might have enhanced homeostatic slow wave occurrence in fronto-central but especially postero-central regions, involved in visual processing (Huber et al., 2013). In fact, most participants selected for sample permutations were recordings made on the second, consecutive day of the experiments.

Further, the explorative aim of the present study motivated a generous FPR set to .01. Six sample permutations and Benjamini–Hochberg-corrected significance thresholds of $\leq .05$ for the three strongest correlates, were performed to test the robustness of correlations. Single deviations from major trends, such as participant 30, severely skewed observed effects, informing about the functional relevance of observed deviations (low scene recognition).

Lastly, it must be highlighted that small-sample correlational studies overall come with considerable risk for both type I and II errors, particularly for the latter (Knudson & Lindsey, 2014). Nonetheless, the statistical power yielded by most of the performed analyses

was well below 80%. Statistical power for Benjamini-Hochberg-corrected memory correlates of parieto-central involvement of slow wave activity amounted to 40%. Likewise, power correlates of scene recognition based on the whole nap period posed a high risk (41-61%) for type II errors: electrode C3 (1-$\beta$ = .61), C4 (1-$\beta$ = .41), P3 (1-$\beta$ = .48).

### 4.5. Conclusion and Future Recommendations

Dimensional reduction of neural signals, using PCA, is anything but a novel technique. In fact, it is widely used: from decomposition of even-related potentials and characterization of cortical involvement to delineation of neural network activities and classification of neuron types (Gouwens et al., 2019; Bernardi et al., 2018; Martínez, Rahsepar, & White, 2017; Bernat, Williams, & Gehring, 2005). Yet, the present study provided novel evidence that such dimensional reduction can be used to study memory processing in the sleeping brain.

On the group-level, the component structure of slow wave activity informed about global, learning-dependent changes in cortical involvement, as shown in comparisons with the work of Bernardi et al. (2018). More importantly, individual differences in this slow wave component structure seemed to reflect the extent of homeostatic slow wave generation and memory consolidation. Indeed, spatial PCA outdoes conventional measures, such as power or power density averages, as it rather informs about abundance than size of slow waves in a given time period. This is crucial, as mainly smaller Type 2 slow waves are shown to respond to learning-dependent changes in homeostatic pressure and proportional release thereof (Bernardi et al., 2018; Tononi & Cirelli, 2014; Mascetti et al., 2013).

Still, many avenues need to be explored. A time-frequency decomposition of main slow wave components should reveal how cortical involvement of slow wave activity develops over a given period. Such an approach would compensate for the lack of temporal resolution in the PCA used here. Further, more rigorous analyses of individual slow waves should inform how exactly variance explained by PCA components relates to abundance of slow waves in a given region. Such an individual approach to slow wave detection and analysis, as adopted by Bernardi et al. (2018), was provided by Mensen, Riedner, and Tononi, (2016). Their Matlab-based toolbox (https://github.com/Mensen/swa-matlab) allows for characterization of individual waves, based on various morphological and topographical features. Nonetheless, spatial PCA may provide a novel tool to assess memory consolidation and learning-dependent changes in slow wave homeostasis, in recordings of sufficient length and electrode density.

## 5. References


Bergmann, T.O., Mölle, M., Diedrichs, J., Born, J., & Siebner, H.R. (2012). Sleep spindle-related reactivation of category-specific cortical regions after learning face-scene associations. *NeuroImage, 59*(3), 2733-2742. doi:10.1016/j.neuroimage.2011.10.036.

Bernat, E. M., Williams, W. J., & Gehring, W. J. (2005). Decomposing ERP time-frequency energy using PCA. *Clinical neurophysiology : official journal of the International Federation of Clinical Neurophysiology, 116*(6), 1314–1334. doi:10.1016/j.clinph.2005.01.019

Boutin, A., & Doyon, J. (2020). A sleep spindle framework for motor memory consolidation. Philosophical transactions of the Royal Society of London. Series B, *Biological sciences, 375*(1799), 232. doi:10.1098/rstb.2019.0232

Cox, R., Schapiro, A. C., Manoach, D. S., & Stickgold, R. (2017). Individual Differences in Frequency and Topography of Slow and Fast Sleep Spindles. *Frontiers in human neuroscience, 11*, 433. doi:10.3389/fnhum.2017.00433

Curcio, G., Ferrara, M., & De Gennaro, L. (2006). Sleep Loss, Learning Capacity and Academic Performance. *Sleep medicine reviews*. 323-337. doi:10.1016/j.smrv.2005.11.001.

de Vivo, L., Bellesi, M., Marshall, W., Bushong, E. A., Ellisman, M. H., Tononi, G., & Cirelli, C. (2017). Ultrastructural evidence for synaptic scaling across the wake/sleep cycle. *Science, 355*(6324), 507–510. doi:10.1126/science.aah5982

Drummond, S. P., Brown, G. G., Gillin, J. C., Stricker, J. L., Wong, E. C., & Buxton, R. B. (2000). Altered brain response to verbal learning following sleep deprivation. *Nature, 403*(6770), 655–657. doi:10.1038/35001068

Dudai, Y., Karni, A., and Born, J. (2015). The consolidation and transformation of memory. *Neuron 88*, 20–32. doi:10.1016/j.neuron.2015.09.004

Ellmore, T.M., Ng, K., Reichert, C.P. (2017). Early and late components of EEG delay activity correlate differently with scene working memory performance. *PLOS ONE 12*(10): doi:10.1371/journal.pone.0186072

Genzel, L., & Wixted, J.T. (2017). Cellular and Systems Consolidation of Declarative Memory in N. Axmacher and B. Rasch (eds.), *Cognitive Neuroscience of Memory consolidation*, (3-16). Switzerland: Springer International Publishing

González-Rueda, A., Pedrosa, V., Feord, R. C., Clopath, C., & Paulsen, O. (2018). Activity-Dependent Downscaling of Subthreshold Synaptic Inputs during Slow-Wave-Sleep-

like Activity In Vivo. *Neuron*, *97*(6), 1244–1252.e5. doi:10.1016/j.neuron.2018.01.047

Gouwens, N. W., Sorensen, S. A., Berg, J., Lee, C., Jarsky, T., Ting, J., Sunkin, S. M., Feng, D., Anastassiou, C. A., Barkan, E., Bickley, K., Blesie, N., Braun, T., Brouner, K., Budzillo, A., Caldejon, S., Casper, T., Castelli, D., Chong, P., Crichton, K., … Koch, C. (2019). Classification of electrophysiological and morphological neuron types in the mouse visual cortex. *Nature neuroscience, 22*(7), 1182–1195. doi:10.1038/s41593-019-0417-0

Iber, C., Ancoli-Israel, S., Chesson, A., & Quan, S. (2007). The AASM manual for the scoring of sleep and associated events: Rules, terminology, and technical specifications. Westchester, IL: American Academy of Sleep Medicine.

Jasper, H. H. (1958). The ten-twenty electrode system of the international federation. *Electroencephalography and Clinical Neurophysiology, 10*, 371–375.

Hebb D.O. (1949). The organization of behavior; a neuropsychological theory. New York: Wiley.

Hirshhorn, M., Grady, C., Rosenbaum, R. S., Winocur, G., & Moscovitch, M. (2012). The hippocampus is involved in mental navigation for a recently learned, but not a highly familiar environment: a longitudinal fMRI study. *Hippocampus, 22*(4), 842–852. doi:10.1002/hipo.20944

Holz, J., Piosczyk, H., Feige, B., Spiegelhalder, K., Baglioni, C., Riemann, D. & Nissen, C. (2012). EEG sigma and slow-wave activity during NREM sleep correlate with overnight declarative and procedural memory consolidation. *Journal of Sleep Research, 21*, 612-619. doi:10.1111/j.1365-2869.2012.01017.x

Huber, R., Felice Ghilardi, M., Massimini, M., & Tononi, G. (2004). Local sleep and learning. *Nature 430***,** 78–81. doi:10.1038/nature02663

Huber, R., Mäki, H., Rosanova, M., Casarotto, S., Canali, P., Casali, A. G., Tononi, G., & Massimini, M. (2013). Human cortical excitability increases with time awake. *Cerebral cortex*, *23*(2), 332–338. doi:10.1093/cercor/bhs014

Knudson, D. V., & Lindsey, C. (2014). Type I and Type II Errors in Correlations of Various Sample Sizes. *Comprehensive Psychology*. doi:10.2466/03.CP.3.1

Langille, J.J. (2019). Remembering to Forget: A Dual Role for Sleep Oscillations in Memory Consolidation and Forgetting. *Frontiers in Cellular Neuroscience, 13*, 71. doi:10.3389/fncel.2019.0007

Lee, S. H., & Dan, Y. (2012). Neuromodulation of brain states. *Neuron, 76*(1), 209–222. doi:10.1016/j.neuron.2012.09.012

Lee, S., & Lee, D. K. (2018). What is the proper way to apply the multiple comparison test?. *Korean journal of anesthesiology, 71*(5), 353–360. doi:10.4097/kja.d.18.00242

Marrosu, F., Portas, C., Mascia, M. S., Casu, M. A., Fà, M., Giagheddu, M., Imperato, A., & Gessa, G. L. (1995). Microdialysis measurement of cortical and hippocampal acetylcholine release during sleep-wake cycle in freely moving cats. *Brain Research, 671*(2), 329–332. doi:10.1016/0006-8993(94)01399-3

Martínez, J. J., Rahsepar, B., & White, J. A. (2017). Anatomical and Electrophysiological Clustering of Superficial Medial Entorhinal Cortex Interneurons. *eNeuro, 4*(5), 263-316. doi:10.1523/ENEURO.0263-16.2017

Mascetti, L., Muto, V., Matarazzo, L., Foret, A., Ziegler, E., Albouy, G., Sterpenich, V., Schmidt, C., Degueldre, C., Leclercq, Y., Phillips, C., Luxen, A., Vandewalle, G., Vogels, R., Maquet, P., & Balteau, E. (2013). The impact of visual perceptual learning on sleep and local slow-wave initiation. *Journal of Neuroscience, 33*(8), 3323–3331. doi:10.1523/JNEUROSCI.0763-12.2013

Massimini, M., Huber, R., Ferrarelli, F., Hill, S., & Tononi, G. (2004). The sleep slow oscillation as a traveling wave. *The Journal of neuroscience : the official journal of the Society for Neuroscience*, *24*(31), 6862–6870. doi:10.1523/JNEUROSCI.1318-04.2004

Mei, N., Grossberg, M. D., Ng, K., Navarro, K. T., & Ellmore, T. M. (2018). A high-density scalp EEG dataset acquired during brief naps after a visual working memory task. *Data in brief*, *18*, 1513–1519. doi:10.1016/j.dib.2018.04.073

Mensen, A., Riedner, B., & Tononi, G. (2016). Optimizing detection and analysis of slow waves in sleep EEG. *Journal of Neuroscience Methods, 274*, 1-12. doi:10.1016/j.jneumeth.2016.09.006.

Miyamoto, D., Hirai, D., & Murayama, M. (2017). The Roles of Cortical Slow Waves in Synaptic Plasticity and Memory Consolidation. *Frontiers in Neural Circuits, 11*, 99. doi:10.3389/fncir.2017.00092

Müller, G. E., & Pilzecker, A. (1900). Experimentelle Beiträge zur Lehre vom Gedächtnis. Leipzig: J.A. Barth.

Nere, A., Hashmi, A., Cirelli, C., & Tononi, G. (2013). Sleep-dependent synaptic down-selection (I): modelling the benefits of sleep on memory consolidation and integration. *Frontiers in neurology*, *4*, 143. doi:10.3389/fneur.2013.00143

Robin, J. & Moscovitch, M. (2017). Details, gist and schema: hippocampal–neocortical interactions underlying recent and remote episodic and spatial memory. *Current Opinion in Behavioral Sciences, 17*, 114-123. doi:10.1016/j.cobeha.2017.07.016.

Sämann, P.G., Wehrle, R., Hoehn, D., Spoormaker, V.I., Peters, H., Tully, C., Holsboer, F., & Czisch, M. (2011). Development of the Brain's Default Mode Network from Wakefulness to Slow Wave Sleep. *Cerebral Cortex, 21*(9), 2082–2093. doi:10.1093/cercor/bhq295

Schmidt, C., Peigneux, P., Muto, V., Schenkel, M., Knoblauch, V., Münch, M., de Quervain, D. J., Wirz-Justice, A., & Cajochen, C. (2006). Encoding difficulty promotes postlearning changes in sleep spindle activity during napping. *The Journal of neuroscience : the official journal of the Society for Neuroscience*, *26*(35), 8976–8982. doi:10.1523/JNEUROSCI.2464-06.2006

Seol, G. H., Ziburkus, J., Huang, S., Song, L., Kim, I. T., Takamiya, K., Huganir, R. L., Lee, H. K., & Kirkwood, A. (2007). Neuromodulators control the polarity of spike-timing-dependent synaptic plasticity. *Neuron*, *55*(6), 919–929. doi:10.1016/j.neuron.2007.08.013

Siclari, F., Bernardi, G., Riedner, B. A., LaRocque, J. J., Benca, R. M., & Tononi, G. (2014). Two distinct synchronization processes in the transition to sleep: a high-density electroencephalographic study. *Sleep*, *37*(10), 1621–1637. doi:10.5665/sleep.4070

Silson, E. H., Steel, A., Kidder, A., Gilmore, A. W., & Baker, C. I. (2019). Distinct subdivisions of human medial parietal cortex support recollection of people and places. *eLife, 8*, e47391. doi:10.7554/eLife.47391

Stern. P. (2018). Synaptic downscaling during “up” states. *Science 360*(6388), 504. doi:10.1126/science.360.6388.504-c

Stickgold, R., & Walker, M. P. (2013). Sleep-dependent memory triage: evolving generalization through selective processing. *Nature neuroscience*, *16*(2), 139–145. doi:10.1038/nn.3303

Tononi, G., & Cirelli, C. (2014). Sleep and the price of plasticity: from synaptic and cellular homeostasis to memory consolidation and integration. *Neuron*, *81*(1), 12–34. doi:10.1016/j.neuron.2013.12.025

van Assche, M., Kebets, V., Vuilleumier, P., Assal, F. (2016). Functional Dissociations Within Posterior Parietal Cortex During Scene Integration and Viewpoint Changes. *Cerebral Cortex, 26*(2), 586–598. doi:10.1093/cercor/bhu215

Verleger, R., Rose, M., Wagner, U., Yordanova, J., & Kolev, V. (2013). Insights into sleep's role for insight: Studies with the number reduction task. *Advances in cognitive psychology, 9*(4), 160–172. doi:10.2478/v10053-008-0143-8

Winkler, I., Debener, S., Müller, K. R., & Tangermann, M. (2015). On the influence of high-pass filtering on ICA-based artifact reduction in EEG-ERP. *Conference proceedings : ... Annual International Conference of the IEEE Engineering in Medicine and Biology Society. IEEE Engineering in Medicine and Biology Society. Annual Conference*, *2015*, 4101–4105. doi:10.1109/EMBC.2015.7319296

Xiao J, Hays J, Ehinger KA, Oliva A, Torralba A, editors. Sun database: Large-scale scene recognition from abbey to zoo. Computer vision and pattern recognition (CVPR), 2010 IEEE conference on; 2010: IEEE.

Zakeri Z., Assecondi S., Bagshaw A.P., Arvanitis T.N. (2014) Influence of Signal Preprocessing on ICA-Based EEG Decomposition. In: Roa Romero L. (eds) XIII Mediterranean Conference on Medical and Biological Engineering and Computing 2013. IFMBE Proceedings, vol 41. Springer, Cham

## 6. Appendices

Appendix A

Electrode placement during EEG measurements with Fpz as ground and TP9 as reference electrodes.

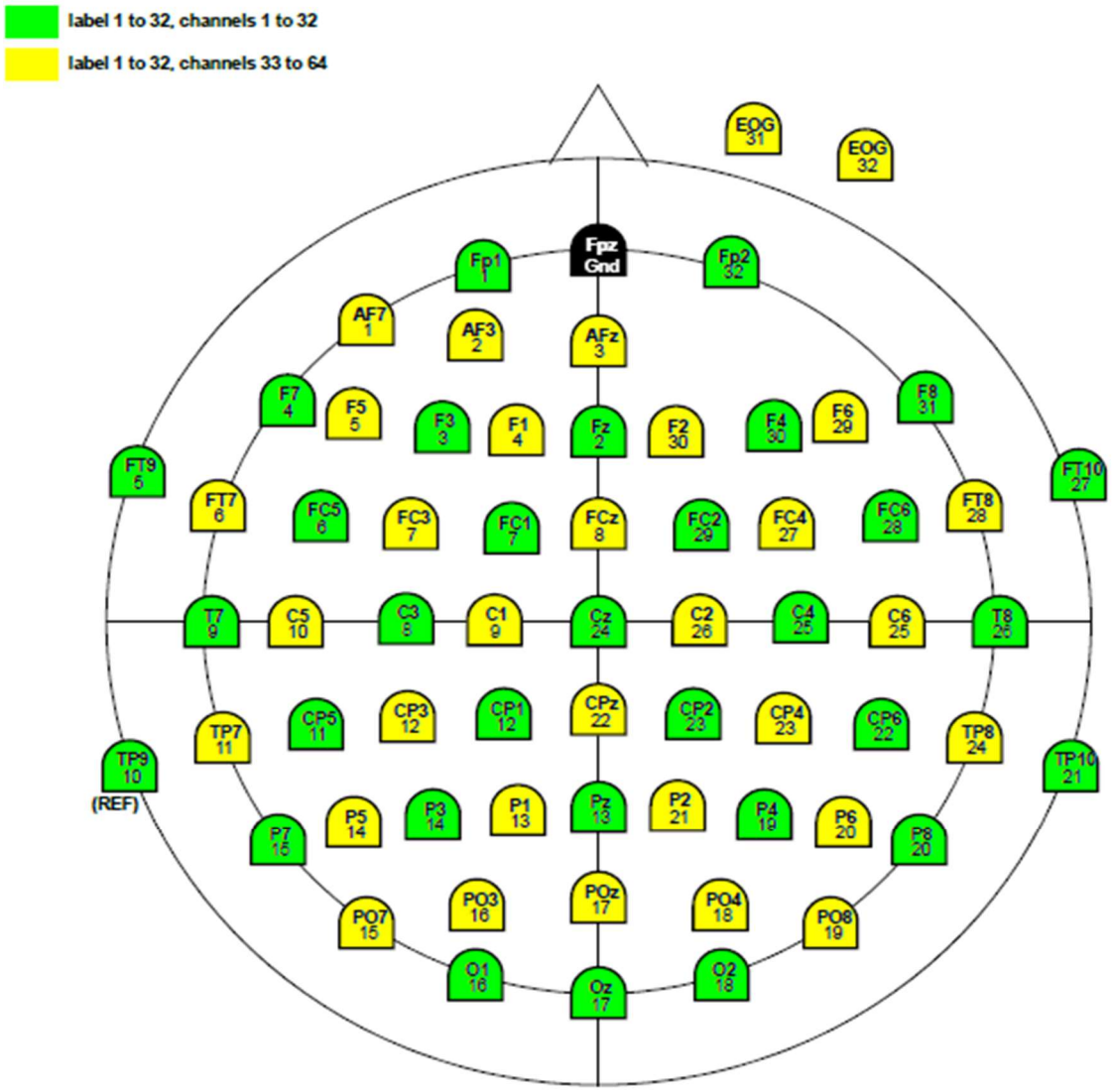

Appendix B

Scatterplots of log-10 slow wave power against scene recognition scores for eight, selected electrodes: F3, F4, C3, C4, P3, P4, O1, O2. Slow wave power (log-10(uV^2)

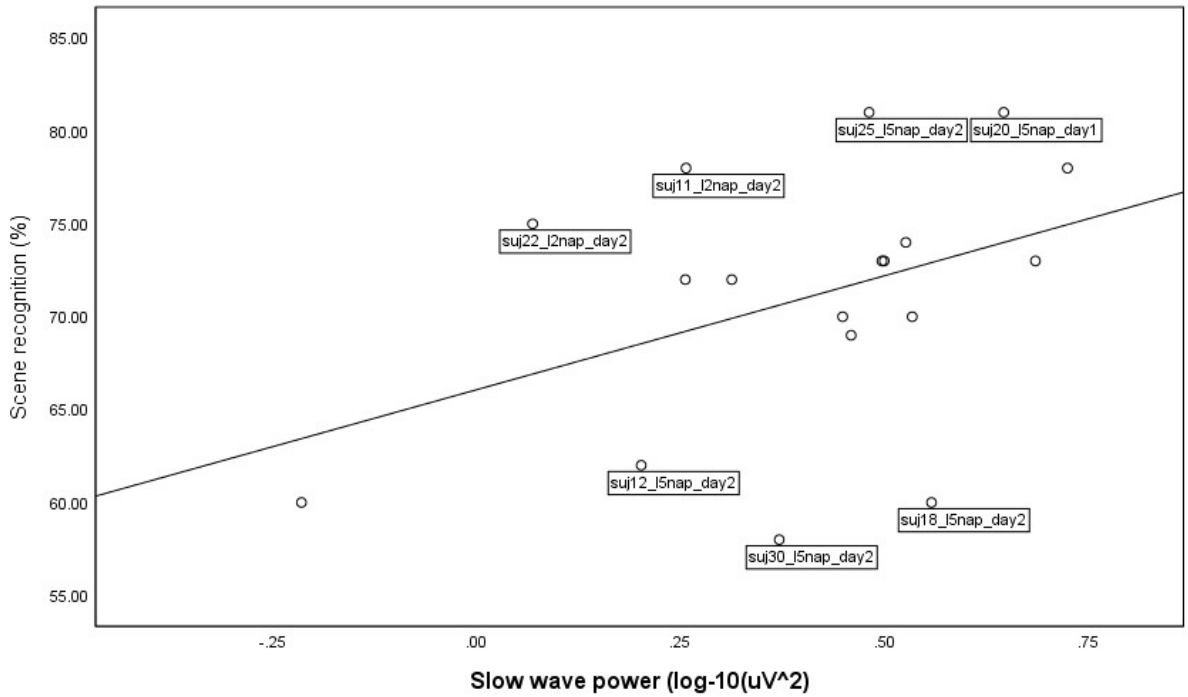


*Figure 1.* Correlations of slow wave power at recordings site F3 averaged across the whole nap with scene recognition.

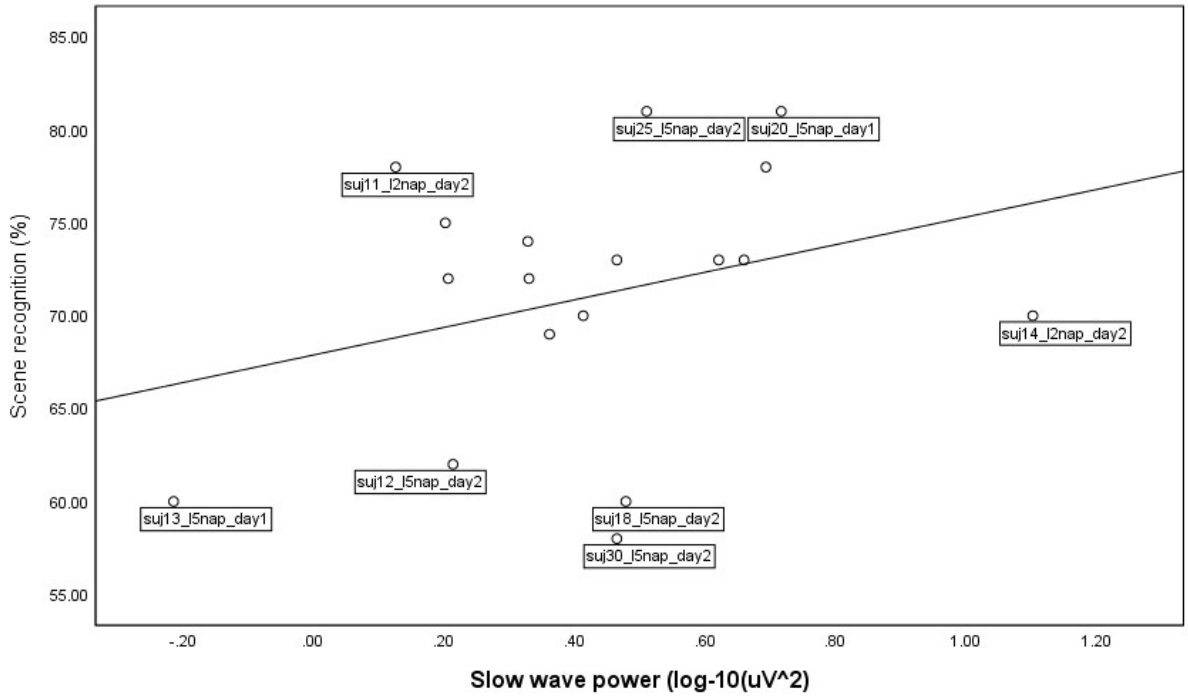


*Figure 2.* Correlations of slow wave power at recordings site F4 averaged across the whole nap with scene recognition.

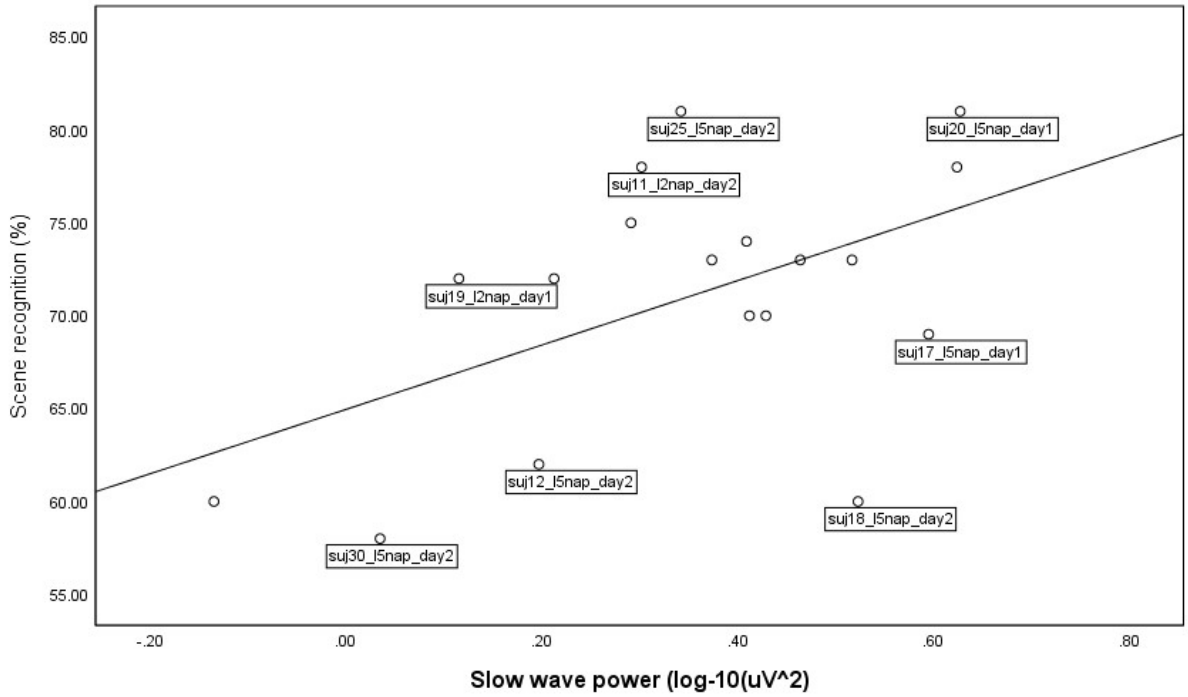


*Figure 3.* Correlations of slow wave power at recordings site C3 averaged across the whole nap with scene recognition.

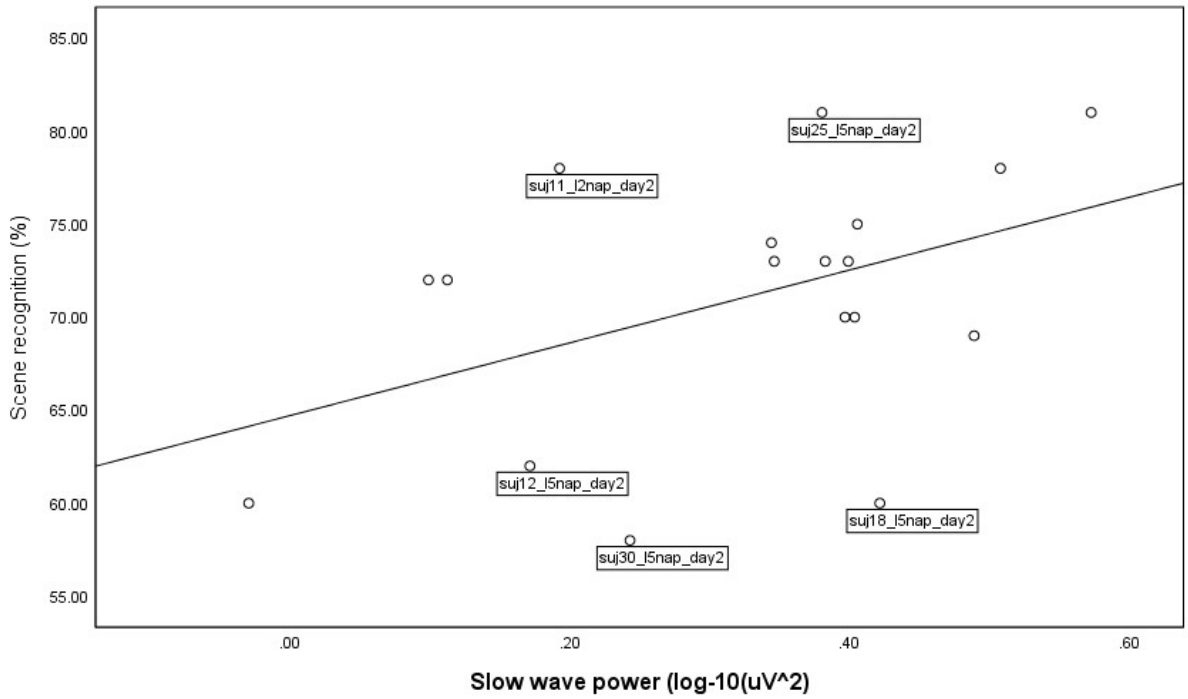


*Figure 4.* Correlations of slow wave power at recordings site C4 averaged across the whole nap with scene recognition.

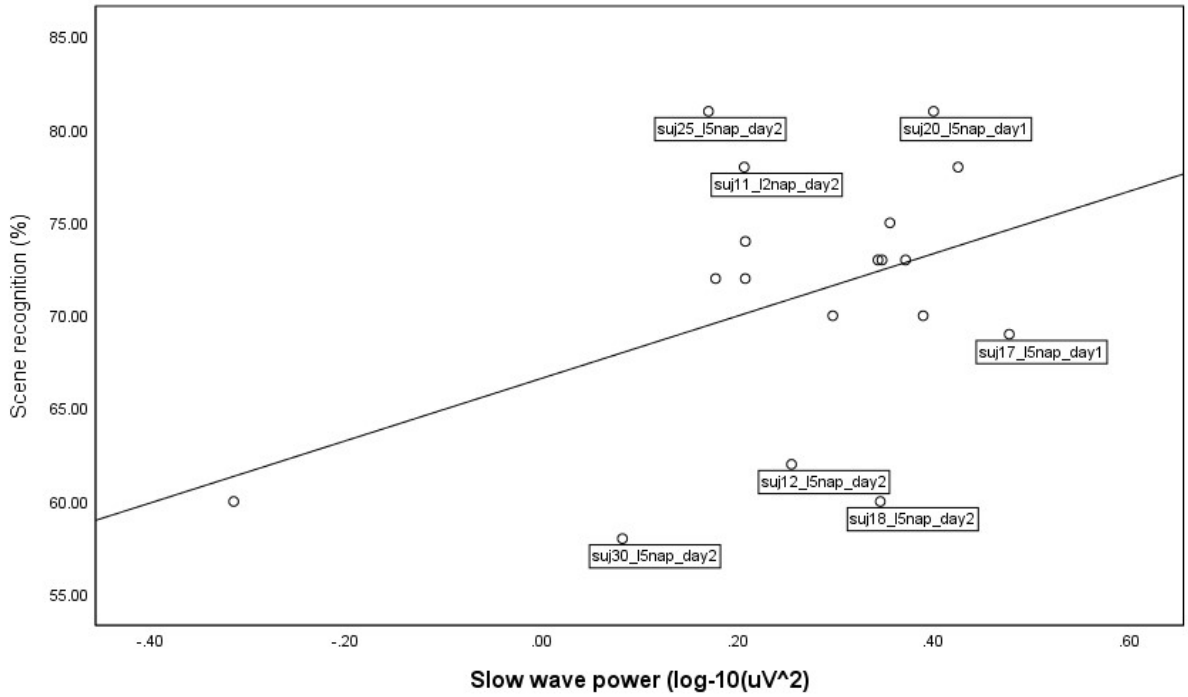


*Figure 5.* Correlations of slow wave power at recordings site P3 averaged across the whole nap with scene recognition.

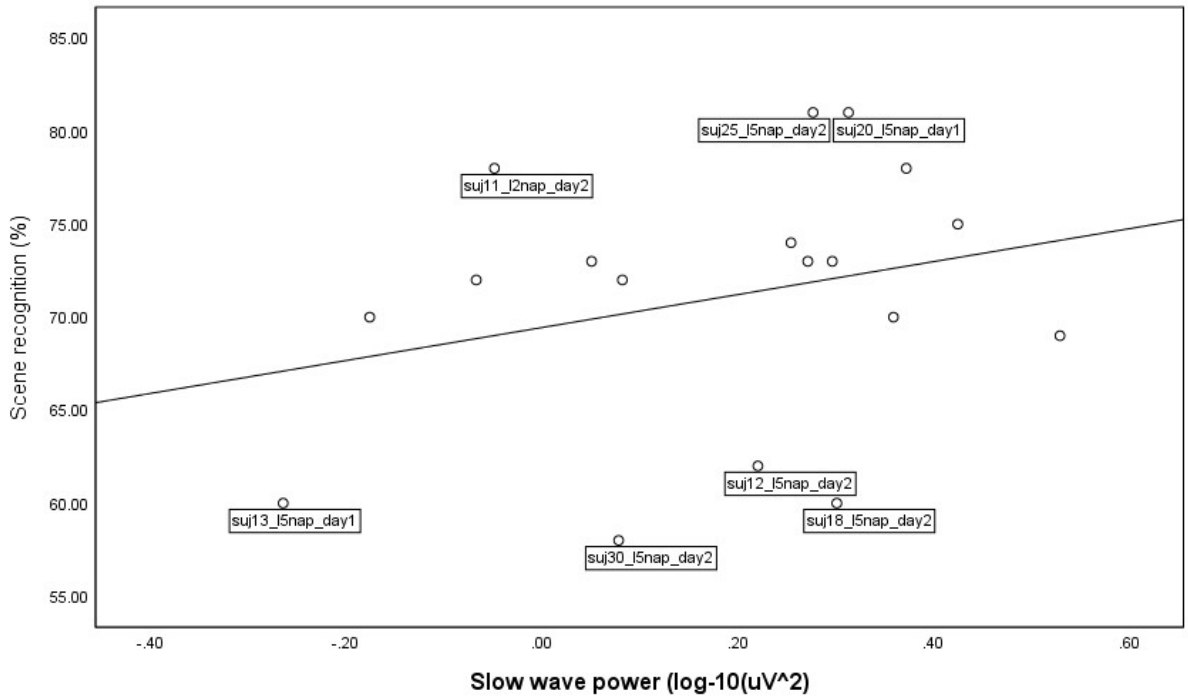


*Figure 6.* Correlations of slow wave power at recordings site P4 averaged across the whole nap with scene recognition.

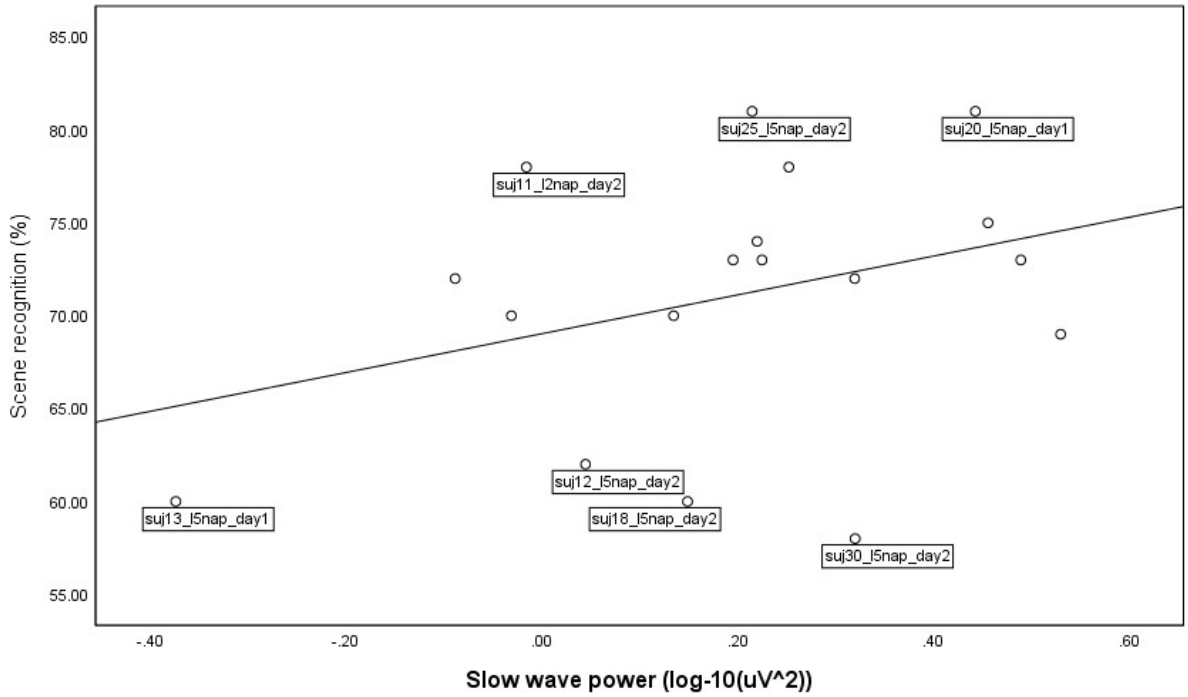


*Figure 7.* Correlations of slow wave power at recordings site O1 averaged across the whole nap with scene recognition.

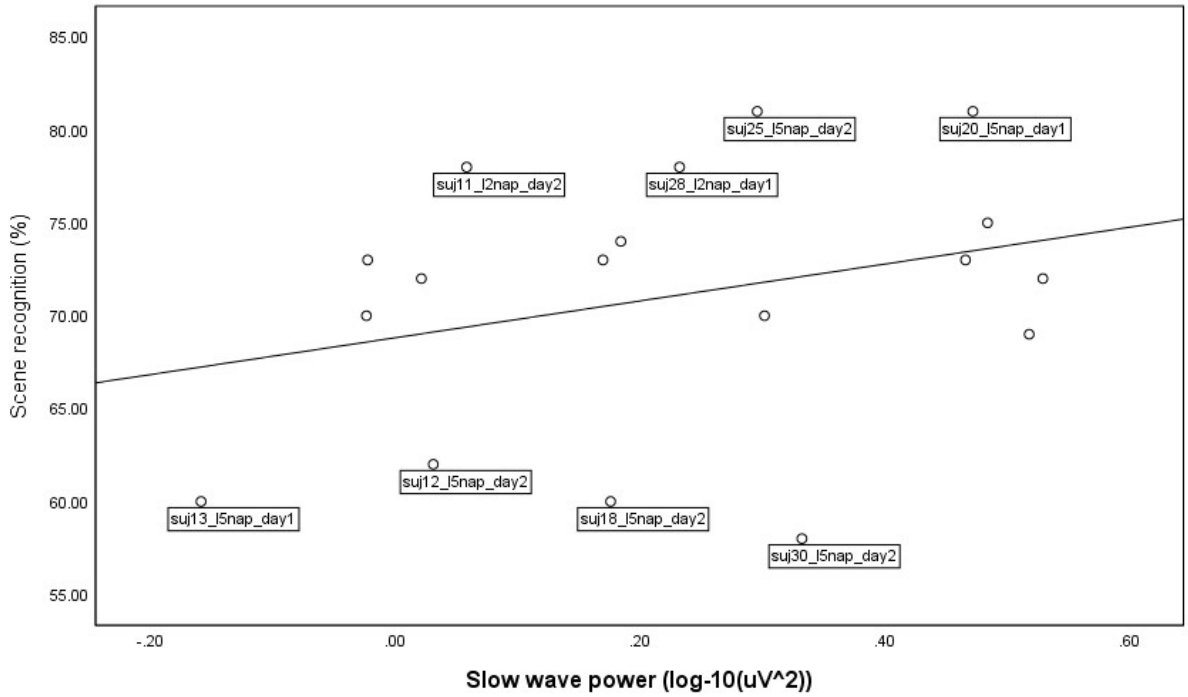


*Figure 8.* Correlations of slow wave power at recordings site O2 averaged across the whole nap with scene recognition.

Appendix C

Scatterplots of the variance explained by the two, prime components of slow wave scalp involvement throughout the nap against scene recognition.

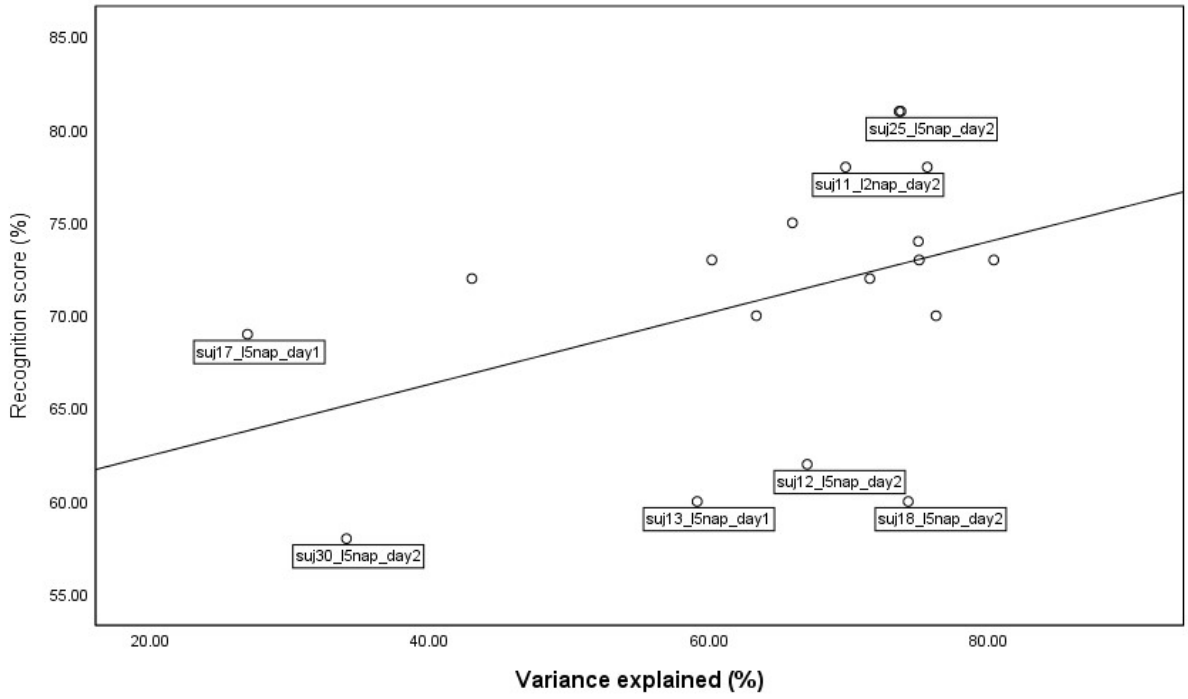


*Figure 1.* Correlations of the variance explained by the biggest postero-central component with scene recognition.

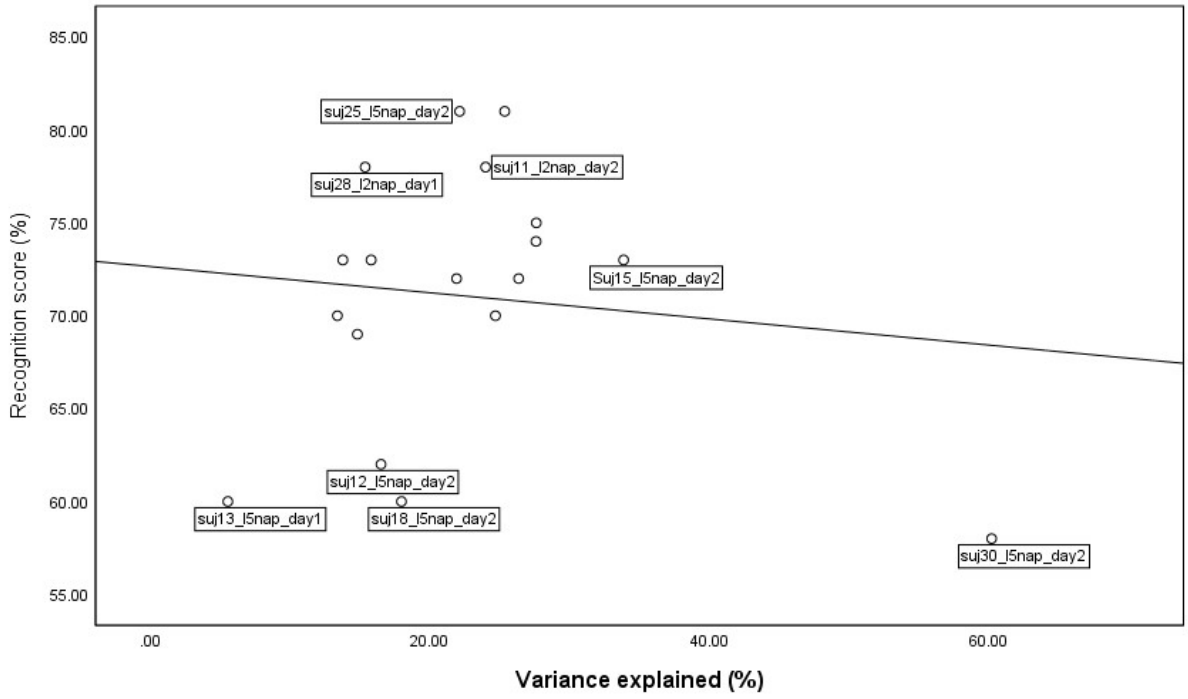


*Figure 2.* Correlations of the variance explained by the second biggest fronto-central component with scene recognition

Appendix D

The dimensional structure of slow wave scalp involvement illustrated on the basis of the first four recordings. Noteworthy, a postero-central component explained most of the variance in slow wave activity, followed by fronto-central and lateralized component.